



Chem Soc Rev

**Catechol-Functionalized Hydrogels: Biomimetic Design,  
Adhesion Mechanism, and Biomedical Applications**

Journal:	<i>Chemical Society Reviews</i>
Manuscript ID	CS-SYN-04-2019-000285.R2
Article Type:	Review Article
Date Submitted by the Author:	18-Dec-2019
Complete List of Authors:	<p>Zhang, Wei; Southeast University, Department of Material Science and Engineering</p> <p>Wang, Ruixing; Southeast University, Department of Material Science and Engineering</p> <p>Sun, Zhengming; Southeast University, Materials Science and Engineering; Sangyo Gijutsu Sogo Kenkyujo Tsukuba Chuo,</p> <p>Zhu, Xiangwei; Huazhong University of Science and Technology, Chemistry and Chemical Engineering</p> <p>Zhao, Qiang; Huazhong University of Science and Technology, Chemistry and Chemical Engineering</p> <p>Zhang, Tengfei; Jiangsu Key Laboratory of Electrochemical Energy-Storage Technologies, College of Materials Science and Technology, Nanjing University of Aeronautics and Astronautics</p> <p>Cholewinski, Aleksander; University of Waterloo, Department of Chemical Engineering</p> <p>Yang, Fut; University of Waterloo, Department of Chemical Engineering</p> <p>Zhao, Boxin; University of Waterloo, Department of Chemical Engineering</p> <p>Pinnaratip, Rattapol; Michigan Technological University, Biomedical Engineering</p> <p>Forooshani, Pegah; Michigan Technological University, Biomedical Engineering</p> <p>Lee, Bruce; Michigan Technological University, Biomedical Engineering</p>

SCHOLARONE™  
Manuscripts

## Catechol-Functionalized Hydrogels: Biomimetic Design, Adhesion Mechanism, and Biomedical Applications

Wei Zhang,<sup>\*a</sup> Ruixing Wang,<sup>a</sup> ZhengMing Sun,<sup>\*a</sup> Xiangwei Zhu,<sup>b</sup> Qiang Zhao,<sup>\*b</sup> Tengfei Zhang,<sup>c</sup> Aleksander Cholewinski,<sup>d</sup> Fut (Kuo) Yang,<sup>d</sup> Boxin Zhao,<sup>\*d</sup> Rattapol Pinnaratip,<sup>e</sup> Pegah Kord Forooshani,<sup>e</sup> and Bruce P. Lee,<sup>\*e</sup>

<sup>a</sup>*Jiangsu Key Laboratory of Advanced Metallic Materials, School of Materials Science and Engineering, Southeast University, Nanjing, 211189, China. E-mail: w69zhang@seu.edu.cn; zmsun@seu.edu.cn*

<sup>b</sup>*Key Laboratory of Material Chemistry for Energy Conversion and Storage, Ministry of Education, School of Chemistry and Chemical Engineering, Huazhong University of Science and Technology, Wuhan 430074, China. E-mail: zhaoq@hust.edu.cn*

<sup>c</sup>*Jiangsu Key Laboratory of Electrochemical Energy-Storage Technologies, College of Materials Science and Technology, Nanjing University of Aeronautics and Astronautics, Nanjing 210016, China*

<sup>d</sup>*Department of Chemical Engineering, Waterloo Institute for Nanotechnology, Centre for Bioengineering and Biotechnology, University of Waterloo, Ontario, Canada N2L 3G1. E-mail: zhaob@uwaterloo.ca*

<sup>e</sup>*Department of Biomedical Engineering, Michigan Technological University, Houghton, Michigan 49931, United States. E-mail: bplee@mtu.edu.*

**Abstract:** Hydrogels are a unique class of polymeric materials that possess an interconnected porous network across various length scales from nano- to macroscopic dimensions and exhibit remarkable structure-derived properties, including high surface area, an accommodating matrix, inherent flexibility, controllable mechanical strength, and excellent biocompatibility. Strong and robust adhesion between hydrogels and substrates is highly desirable for their integration into and subsequent performance in biomedical devices and systems. However, the adhesive behavior of hydrogels is severely weakened by the large amount of water that interacts with the adhesive groups reducing the interfacial interactions. The challenges of developing tough hydrogel-solid interfaces and robust bonding in wet conditions are analogous to the adhesion problems solved by marine organisms. Inspired by mussel adhesion, a variety of catechol-functionalized adhesive hydrogels have been developed, opening a door for the design of multi-functional platforms. This review is structured to give a comprehensive overview of adhesive hydrogels starting with the fundamental challenges of underwater adhesion, followed by synthetic approaches and fabrication techniques, as well as characterization methods, and finally their practical applications in tissue repair and regeneration, antifouling and antimicrobial applications, drug delivery, and cell encapsulation and delivery. Insights on these topics will provide rational guidelines for using nature's blueprints to develop hydrogel materials with advanced functionalities and uncompromised adhesive properties.

## 1 Introduction

Hydrogels—three-dimensionally interconnected hydrophilic polymer chains—are capable of absorbing and retaining large amounts of water in their networks.<sup>1–4</sup> They can swell extensively without dissolution owing to the presence of chemical or physical cross-links, which provide a network structure and maintain macroscopic integrity.<sup>5</sup> Chemical cross-links are formed via covalent bonds that are commonly initiated by free radical polymerization or metal-mediated chelation, while physical cross-links include hydrogen bonding, hydrophobic interactions, ionic interactions, or crystallites.<sup>6,7</sup> Depending on the cross-linking mechanism and the nature of the functional groups, hydrogels can be tailored to have varied porous structure, mechanical resistance, and an ability to transport solvents. Moreover, they can be further tuned toward the integration of functional components or chemically/biologically active systems, such as stimuli-responsive molecules, electrically conductive fillers, or adhesive moieties.<sup>8–11</sup> For example, when a hydrogel is composited with electro-active materials, it presents a desirable framework for constructing flexible energy storage devices.<sup>12</sup> In addition, stimuli-responsive moieties allow hydrogels to perform on-demand volume/shape transitions in response to external conditions such as pH, temperature, an electric or magnetic field, and light.<sup>13</sup> The remarkable versatility in the design of their electrical, mechanical, and optical properties has endowed hydrogels with widespread applications, such as biomedical adhesives and artificial skin, as well as drug delivery and bio-electronics.<sup>14,15</sup>

A significant amount of work has been carried out to investigate the mechanical and chemical properties of functional hydrogels as well as their applications.<sup>4,16</sup> Several reviews are available on the preparation and functionalization of composite hydrogels containing various fillers, including carbon nanotubes and graphene sheets, conductive polymers, and inorganic nanoparticles.<sup>13,17</sup> Some reviews are dedicated to specific applications such as bioelectronics or drug delivery;<sup>18,19</sup> our recent work discussed the development of electrically conductive and mechanically robust hydrogels for flexible energy storage applications.<sup>12</sup> Despite remarkable growth in the number of advanced hydrogels reported in recent years, many opportunities remain unexplored. Strong and robust adhesion between hydrogels and solid materials in wet conditions, which is highly desirable for their integration into and performance in devices and systems, remains an ongoing challenge in the field.<sup>20–22</sup> The search for general and practical strategies for achieving tough hydrogel bonding to diverse surfaces has prompted researchers to explore their unique properties and fundamental mechanisms.

The adhesive behavior of hydrogels is severely weakened by the large amount of water in their polymer network, as water creates a weak boundary layer that can prevent direct surface contact between the hydrogels and substrates, leading to diminished surface energy and deterioration of the adhesion strength.<sup>23–27</sup> Moreover, the water molecules interact with the adhesive groups in the hydrogels via hydrogen bonding, which significantly reduces the interfacial reactions between the hydrogels and solid materials. This situation is complicated further when hydrogels are applied in biomedical engineering where most surfaces (human bodies, tissues, and biogluers) are wet and soft.<sup>28,29</sup>

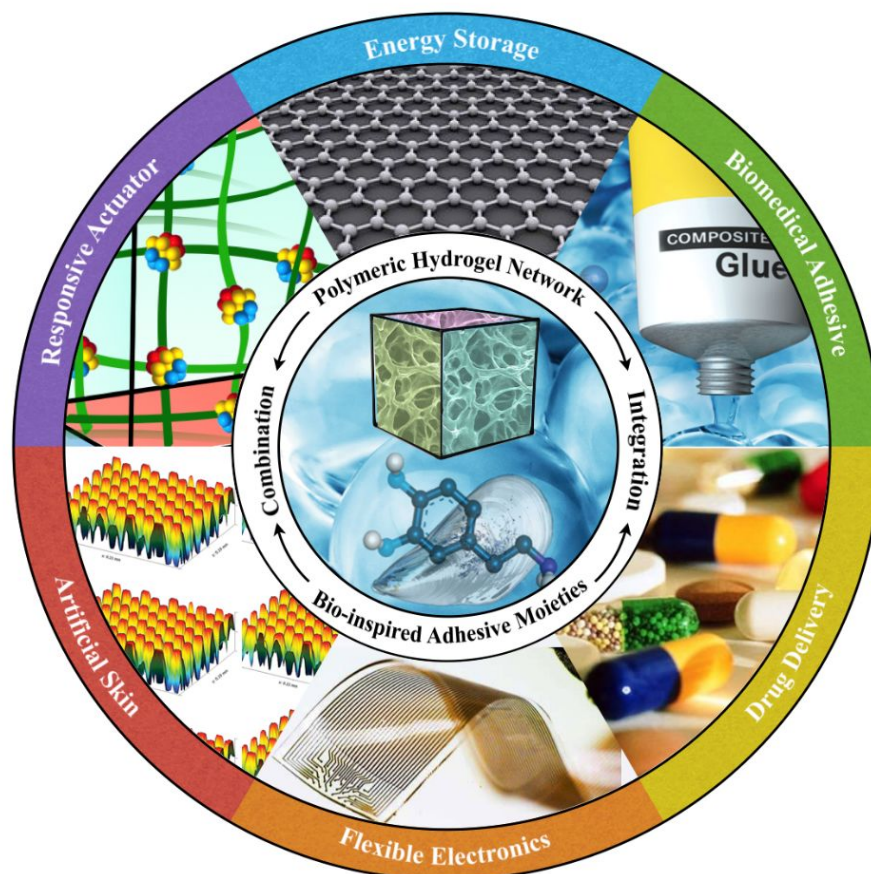


**Figure 1.** Design and development of adhesive hydrogels based on biomimetic principles, and their potential applications in a wide range of fields.

The challenges of developing tough and robust underwater bonding are analogous to the adhesion problems solved by marine mussels, which are naturally equipped with reliable strategies to achieve interfacial adhesion in dynamic and turbulent environments.<sup>27,30–32</sup> 3,4-dihydroxy-L-phenylalanine (DOPA), a catecholic amino acid present in mussel adhesive proteins, has been identified as being able to penetrate water boundary layers, and subsequently interacts with local metal ions to form adhesive bonds with substrates.<sup>33–35</sup> As a result, the catechol moieties of DOPA have been exploited as a popular inspiration for the design of biomimetic wet adhesives.<sup>36,37–41</sup> Developing novel adhesive hydrogels based on biomimetic principles may have significant implications for understanding the fundamentals of underwater adhesion. Beyond exploring the chemistry, the intrinsic properties of adhesive hydrogels have paved the way for the design of new (multi)functional platforms.<sup>42–45</sup> Therefore, a thorough understanding of these systems is needed if we wish to use nature's blueprints to develop the next generation of biomedical materials.

In this review, we develop three interconnected themes, including how water undermines adhesion in hydrogels; how biomimetic adhesives and coatings work; and how basic research in this area has translated hydrogels to diverse applications. Each of these themes has attracted tremendous interest in recent years; the associated research challenges involve broad and in depth

interdisciplinary questions, including not only biology and chemistry, but also materials science, surface engineering, and polymer science. We start with a brief overview of the fundamental mechanisms of hydrogel adhesion, then we comment on commonly used characterization methods used to investigate the adhesion strength of hydrogels, with the hope that it will provide some guidance for establishing the experimental setup and assessment of hydrogel adhesion performance with respect to their swelling or deformation behaviors. Thereafter, we describe synthetic approaches and fabrication techniques for adhesive hydrogels inspired by marine organisms and then discuss their respective applications. By highlighting the unique properties of adhesive hydrogels, we hope to present new insights not only into the fundamental challenges of wet adhesion, but also into the practical applications of robust hydrogel-solid interfaces in diverse areas.

## 2 Hydrogel adhesion: surface energy, intermolecular interactions, and near-surface effects

### 2.1 The heterogeneous nature of hydrogels

When considering the adhesion and surface energy of hydrogels, their heterogeneous nature is an important factor. Hydrogels consist of both water and polymer; these two components each play an important role in either enhancing or reducing adhesion. The exact nature of their roles (particularly for water) depends on the environment of the gel and the interactions between the components. While a hydrogel may adhere poorly to a hydrophobic surface in air, it can adhere well to a hydrophilic surface. As illustrated in Fig 2, when a hydrogel is placed onto a hydrophilic surface, water can flow out of the gel to wet the surface, forming a water meniscus at the edges of the contact region. In addition to the intermolecular interactions within the contact region, the capillary adhesion increases the force required to pull away the hydrogel. In contrast, when a hydrogel is applied to a surface submerged in water, pressure is normally required to remove the free water at the surface, and adhesion primarily occurs as a result of the interactions between the polymer chains and the surface.

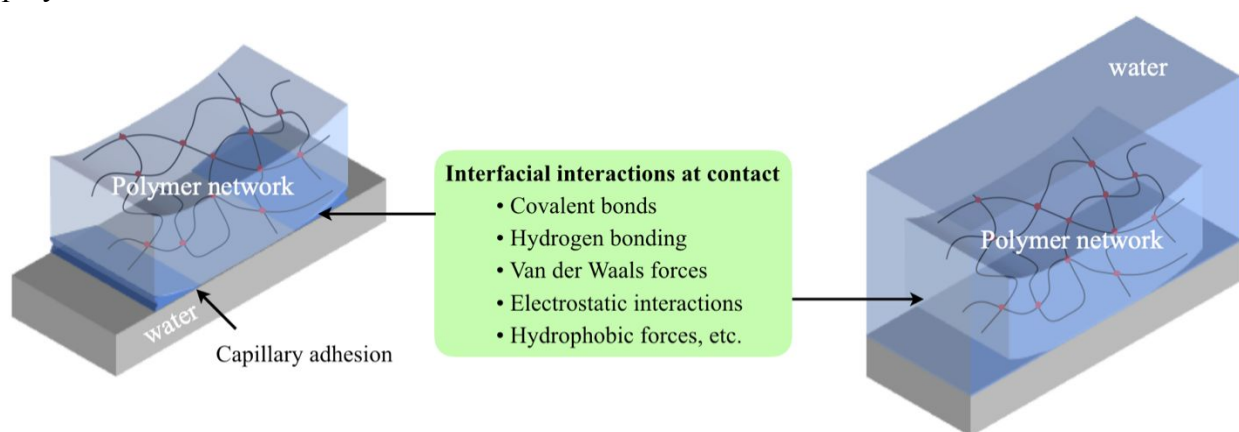


**Figure 2.** Hydrogel adhesion in air (left panel) and in water (right panel), and typical interfacial interactions at the contact points.

Because of the heterogeneous nature of hydrogels and the dynamic interactions with their environments, the observed adhesion of hydrogels is far less understood than the behavior of pure liquids and solids. It is helpful to consider hydrogel adhesion from three different perspectives: (a) surface energy and work of adhesion, (b) intermolecular interactions at the interface, and (c) near-surface phenomena that can influence adhesion.

## 2.2 Hydrogel surface energy and work of adhesion

The surface energy is a useful concept for adhesion; it is related to the work of adhesion ( $W_A$ ) by the equation:

$$W_A = \gamma_1 + \gamma_2 - \gamma_{12} \quad (1)$$

where  $\gamma_1$  and  $\gamma_2$  are the surface energies of the two contacting surfaces, and  $\gamma_{12}$  is the interfacial energy between the surfaces. The surface energy of a hydrogel is a result of its nature as a chemically heterogeneous surface. As such, it is dependent on the surface energy of the polymer, the surface tension of water, and the relative fraction of each component. Despite the extensive study of hydrogel materials, no suitable theoretical framework for determining the surface energy of gels from their components has been established. As a first approximation, the overall surface energy of the hydrogel is related to the individual components in a similar manner to Cassie's law, which uses a linear combination of the surface energies of a heterogeneous system, weighted by their relative fractional area.<sup>46</sup> As such, the surface energy of a gel,  $\gamma_{gel}$ , can be written

$$\gamma_{gel} = \phi_s \gamma_{network} + (1 - \phi_s) \gamma_{water} \quad (2)$$

where  $\gamma_{network}$  is the surface energy of the polymer network in the fully hydrated state,  $\gamma_{water}$  is the surface tension of water, and  $\phi_s$  is the surface fraction of the polymer and is a function of the polymer content and the swelling ratio of the gel. Because the polymer content is only a small fraction of the gel, the surface energy of the gel is approximately the same as that of the water, e.g.,  $\gamma_{gel} \approx \gamma_{water}$  for  $\phi_s \approx 0$ . Experimentally, the effective surface energy of a hydrogel can be determined using captive bubble contact angle measurements. As discussed by Andrade et al.,<sup>47</sup> the surface tension of the dispersive and polar components of a hydrated solid can be estimated using a water-immiscible liquid (e.g., octane) and an air bubble. Nakamura et al.<sup>46</sup> studied the surface tension of poly(N-isopropylacrylamide) gel and polyacrylamide gel using air bubble tests and indeed observed that the gel surface tension is very close to that of water when the temperature is less than the volume phase transition temperature of poly(N-isopropylacrylamide), where the polymer chains are in their hydrated state. Above the volume phase transition temperature of poly(N-isopropylacrylamide), the surface concentration of the polymer chains (now in a dehydrated state) has a dominant effect on the surface tension of the gel.

## 2.3 Interfacial interactions at the contact point

Most adhesives utilize numerous noncovalent interaction points, which are applicable to a broad variety of adherends; these noncovalent interaction points are weak individually but could be strong collectively. These noncovalent interactions include van der Waals forces, electrostatic

forces, hydrogen bonding, and hydrophobic interactions. Van der Waals forces are the most general of these, resulting from fundamental interactions such as permanent, instantaneous, and induced dipole interactions. They are responsible for many forms of adhesion in air, such as lizard geckos which utilize van der Waals interactions to stick to surfaces.<sup>48,49</sup> However, these interactions are significantly weakened by water, and so are less useful for hydrogel adhesion.

Electrostatic forces are also quite nonspecific, relying on charges for attraction. These forces are defined by Coulomb's law:

$$F = \frac{q_1q_2}{4\pi\epsilon r^2} \quad (3)$$

where  $q_1$  and  $q_2$  are the signed magnitudes of two point charges,  $r$  is the distance between them,  $F$  is the force between them (where a negative force indicates attraction), and  $\epsilon$  is the permittivity of the medium. In hydrogel systems, electrostatic forces can be responsible for the structure of the gel itself, such as ionic cross-linking of calcium alginate gels.<sup>50,51</sup> For adhesion, electrostatic interactions can be used to adhere two hydrogels with oppositely charged polymer networks,<sup>52,53</sup> and can also be used in the general adhesion of hydrogel systems.<sup>54</sup>

Electrostatic and van der Waals forces are inversely proportional to the permittivity (or dielectric constant) of the medium (in the case of electrostatic forces,  $\propto 1/\epsilon$ ) or its squared value (for van der Waals forces,  $\propto 1/\epsilon^2$ ).<sup>55</sup> In the case of hydrogels the medium is water, which has a dielectric constant approximately 80 times that of air. As such, the majority of hydrogel adhesive interactions will, at best, be only 1/80 of what they would be in air, leading to a severe weakening of their adhesive properties.

Another form of nonspecific interaction is hydrophobic interactions, which are generally based around nonpolar molecules. They arise as a result of the high entropy cost of water organizing itself around hydrophobic materials. Because of their poor compatibility with water, hydrophobic surfaces are able to repel water molecules when they are brought together, and their interactions are strengthened by the presence of H<sub>2</sub>O as the medium. Their use in adhesion is somewhat limited since hydrogels are primarily hydrophilic. However, it is possible to take advantage of hydrophobic interactions with the presence of certain functional groups on the polymer chains. For example, mussel foot proteins are able to adhere to hydrophobic surfaces by utilizing hydrophobic interactions. This is through hydrophobic side chains as well as catechol functionality.<sup>56</sup> Catechol binds to surfaces in a variety of ways, ranging from hydrophobic interaction and coordination bonding, to covalent bond formation. When adhering to hydrophobic surfaces, catechol can orient itself so that its aromatic ring interacts with the surface, resulting in hydrophobic interactions between the two surfaces.<sup>57</sup>

While many nonspecific interactions are utilized in adhesion, interactions with greater specificity are frequently used to improve the adhesive capabilities of hydrogels. One of the most straightforward approaches is the use of covalent bonding, where functional groups on the polymer chains are chemically reacted with groups on the target surface. Covalent bonds involve the sharing of electrons—where orbitals of the corresponding atoms overlap—and are stronger than physical interactions. However, using covalent bonding for adhesion is often surface-dependent or requires

surface modification. For example, Yuk et al.<sup>38</sup> achieved high interfacial toughness by chemically modifying surfaces to covalently bond to the polymer network in a tough hydrogel. Coordination bonds are another form of covalent bond that can form between hydrogels and metal ions or a metal oxide surface. This can make them an attractive choice for strong and reversible cross-links within a gel. However, for adhesion, owing to the specific surface requirements, coordination is typically used alongside other interactions as part of an adhesive strategy.

Hydrogen bonding is a particular form of dipole-dipole bond involving a hydrogen atom bound to a more electronegative atom/group and another electronegative atom/group with a lone pair.<sup>58</sup> Hydrogen bonds are stronger than many other physical bonds such as van der Waals forces, but are weaker than covalent bonds. While hydrogen bonds are useful for adhesion, water is itself capable of hydrogen bonding. If the hydrogen bonds that water forms with the hydrogel or surface are stronger than those formed between the hydrogel and surface, it is difficult for the two surfaces to interact at all. Some forms of hydrogen bond are stronger than those of water, and hence are good candidates for enhancing underwater adhesion. When catechol binds to a surface through hydrogen bonding, it is able to form bidentate hydrogen bonds; these interactions are stronger and more stable than those of water, meaning that catechol groups can displace water molecules from the surface.<sup>59</sup> Many investigations have used catechol functionality and its versatility in bonding to introduce adhesion into hydrogels<sup>35</sup> and are discussed further in later sections.

Another interaction that has been used in adhesion is supramolecular host-guest chemistry, in which the recognition between the host and guest molecules is able to displace water molecules to form a supramolecular complex.<sup>60</sup> For example, Ahn et al.<sup>61</sup> exploited the ultrahigh affinity between a particular host-guest pair to develop a supramolecular “velcro” with reversible and switchable underwater adhesion. While this example does add reversible and switchable properties to adhesion, it is similar to covalent bonds in requiring modification of the surface.

## 2.4 Near-surface phenomena and bulk effects influencing hydrogel adhesion

When considering hydrogel adhesion, interfacial interactions at the surface are not the only contributors to the overall adhesion; interactions near the surface and within the gel itself also play important roles, particularly in terms of energy dissipation. The ability to dissipate energy can greatly hinder crack propagation at the interface and within the gel itself, increasing the energy required for detachment. In general, the fracture energy ( $G$ ) when an adhesive joint fails is dependent on both the surface energy ( $G_0$ , which represents either  $W_A$  or the work of cohesion  $W_C$ , depending on the mode of failure), as well as other processes that absorb energy ( $\psi$ ), such as plastic and viscoelastic deformation.<sup>62</sup> The relationship between practical ( $G$ ) and fundamental or interfacial ( $G_0$ ) adhesion can be expressed by

$$G = G_0 + \psi \quad (4)$$

While  $\psi$  is typically much larger than  $G_0$ , the two are interconnected, such that  $\psi$  tends to become larger as  $G_0$  increases. The two terms are more directly linked in systems where  $\psi$  is primarily associated with viscoelastic loss (this typically includes hydrogels), such that the equation for  $G$  can be rewritten as



$$G = G_0[1 + f(R,T)] \approx G_0f(R,T), \quad (5)$$

where  $f(R,T)$  is a rate- and temperature-dependent function describing energy dissipation.<sup>63,64</sup> This relationship has been applied to improve overall adhesion by modifying bulk properties. For instance, Yuk et al.<sup>13</sup> formed tough adhesive hydrogels using covalent bonds for adhesion and a double network tough hydrogel for energy dissipation and enhanced adhesion strength. Rao et al.<sup>65</sup> used a tough hydrogel in combination with their adhesive strategy to enhance bulk energy dissipation and delay crack propagation. Karami et al.<sup>66</sup> adapted this strategy, using both fiber reinforcement and a physically cross-linked network to reinforce a chemically cross-linked polymer. The high aspect ratio of the fibers and their ability to penetrate materials resulted in improved adhesion, and the dissipative interface from the fibers and physically cross-linked network led to high interfacial toughness, resulting in high resistance to interfacial crack propagation.

Interactions between water molecules and the polymer network—combined with the porosity of this network—are also important factors in the adhesion of a gel.<sup>6</sup> This is because liquid water is the majority component of hydrogels, but does not transmit force well unless the liquid components are frozen, as recently demonstrated by Yang et al.<sup>67</sup> This is particularly true for free water, which does not interact strongly with the polymer network and behaves like bulk water. However, water molecules that interact more strongly with the polymer chains can become bound.<sup>68</sup> While it is still unclear how these bound molecules influence the properties of the gel, the fraction of free water results in a large component of the gel that does not contribute to underwater adhesion. As such, while the polymer makes up the minority of the hydrogel, it must carry the entire burden of adhesion through interactions with the adherend. These interactions are therefore fewer in number as a result of the low proportion of polymer, leading to a reduction in their overall strength across the entire interface.

On the scale of the entire surface, for a hydrogel sufficiently swollen with water or entirely submerged underwater, interactions between water and the hydrogel polymer (or water and the other adherend) can lead to a boundary layer of water on the surface. If the adhesive components are not able to displace this boundary layer, then there is no direct contact between the adhesive and the adherend.<sup>69</sup> In this situation, water acts as a “weak boundary layer” similarly to other contaminants on a surface that may block adhesion, such as dirt, oil, or oxides. When this occurs, the adhesion of the system is limited by the cohesive strength of this boundary layer, leading to a weak upper bound to the adhesive strength.<sup>70</sup>

To investigate ways to reduce the effects of the water barrier layer, researchers manipulated the physical structure of hydrogels. Inspired by tree frogs and clingfish, rough and structured hydrogels were fabricated; this surface structure encourages the drainage of liquid, removing water from the interface and preventing it from acting as a boundary layer.<sup>65,71</sup> While this does not provide adhesion on its own, it does remove some of the barriers to underwater adhesion for other types of surface forces. Bradley et al.<sup>71</sup> used structured surfaces for drainage in combination with hydrophobic and van der Waals forces to achieve underwater adhesion. Rao et al.<sup>65</sup> used surface structure to encourage drainage and hinder crack propagation, allowing ionic and hydrogen bonds

to establish adhesion. Michel et al.<sup>72</sup> also demonstrated the importance of draining the interface by using superabsorbent hydrogel membranes.

Other factors influencing underwater adhesion exist at the level of the structure of the polymer network or—macroscopically—of the gel itself. When the surface is a porous network, a secondary polymer network can be formed in topological entanglement with both the gel and the surface. Earlier reports achieved this by diffusion and subsequent polymerization and cross-linking of monomer components.<sup>73–75</sup> Recent work by Tamesue et al.<sup>76</sup> has extended this to temperature- and pH-responsive “thread” polymers, as well as application through oxidation-based polymerization, resulting in redox-responsive adhesion. In contrast, Yang et al.<sup>77</sup> have accomplished this through the addition of uncross-linked polymer that can diffuse and cross-link when exposed to a trigger (pH, in the example given). This solution avoids any potential issues related to unreacted monomers that may remain in the gels.

### 3 Experimental methods for measuring hydrogel adhesion

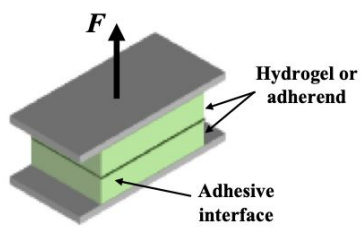
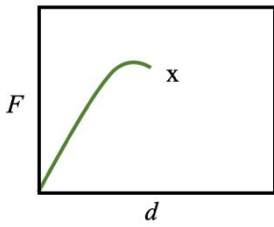
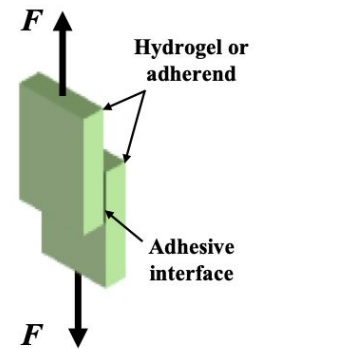
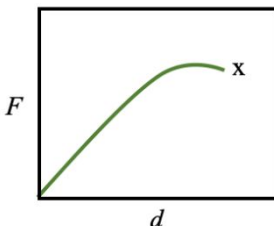
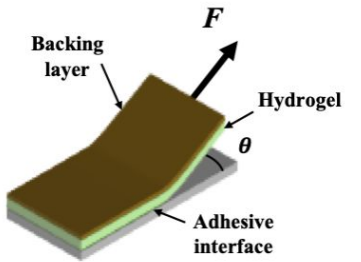
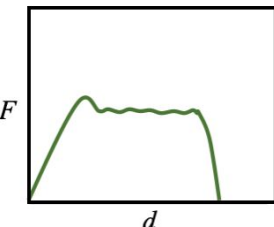
Hydrogel adhesion can be characterized in terms of adhesive strength and adhesive toughness. Adhesive strength gives a measurement of the maximum force per unit area, while adhesive toughness provides information on the amount of energy per unit area required to advance separation.<sup>78</sup> These values correlate to the mechanical properties of the hydrogel and typically need to be optimized for a desired application. A variety of methods for measuring hydrogel adhesion have been reported, varying across the field. Part of the source of this variance is how the detachment can differ depending on the geometry. For instance, the debonding of a tissue adhesive is of a different nature from the peeling of an adhesive patch, which is itself different to the failure of a sealant gel at a burst pressure. Table 1 lists several common techniques for analyzing hydrogel adhesion, including the schematic geometry, force-displacement curve, typical use situations, and example relevant literature. We divide them arbitrarily into two groups. The first group is mainly for evaluating practical adhesion for comparative examination. As mentioned in section 2, this practical adhesion is dependent on both the interfacial adhesion and the bulk properties of the gel. The second group, based on contact mechanics, can examine interfacial adhesion, as well as providing additional insight into the material properties of the hydrogel, e.g., the elastic modulus, work of adhesion, or surface energy, as well as time-dependent behaviors such as stress relaxation and adhesion hysteresis.

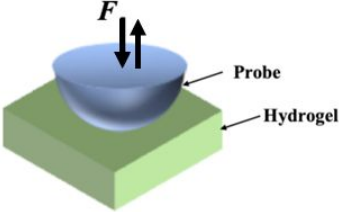
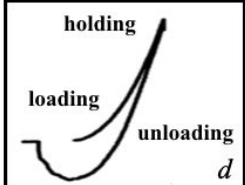
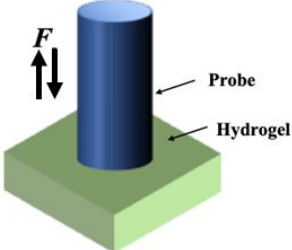
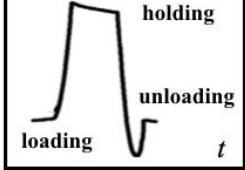
#### 3.1 Evaluation of practical adhesion

Testing methods for evaluating adhesion primarily differ in two ways: (a) in their geometry, and (b) in the adhesive property being tested (typically adhesion strength versus toughness). The tensile pull-off test is one common technique for evaluating adhesive bonding strength. The testing geometry consists of two adherends joined together (either providing adhesion directly, or with a separate adhesive component in between). These surfaces are then pulled apart in a direction normal to their interface. The tensile force can be measured over the displacement until a maximum pull-off force is reached and separation occurs. This pull-off force

can be normalized against the area of contact to acquire the strength in units of pressure. While energy can be obtained from the area under a force-displacement curve, tensile testing is typically used to obtain this pull-off force, which gives an indication of the adhesive strength. For hydrogels, tensile adhesion tests are most often carried out when the hydrogel is acting as a glue, whether to bond together inorganic surfaces<sup>79</sup> or as a tissue adhesive.<sup>54</sup> In the lap shear adhesive test, two surfaces are joined together by overlapping a finite area. In contrast to the tensile test, the joint is pulled apart in a direction parallel to their interface, giving a maximum separation force. The shear adhesive strength is determined by dividing the maximum separation force by the contact area. For hydrogels, this method has been used for both situations where the hydrogel is a middle adhesive component or one of the two adherends. Lap shear tests are more often used for assessing the adhesive strength of a hydrogel film attached to itself or another surface.<sup>66,71</sup> Overall, tensile and lap shear adhesion tests provide complementary information about the adhesive strength tested in different conditions and geometries.

**Table 1.** List of common adhesive testing methods, their respective geometries, representative force-displacement/time curves, typical use situations, and example references in which they are used.

Name	Geometry	F-D curve	Usage situation	Refs
Tensile test			Adhesion strength evaluation in normal direction	51,54
Lap shear test			Adhesion strength evaluation in shear direction	61,71
Peeling test			Adhesion energy and average peel force evaluation at a finite angle and speed	74,76,80-82

Probe-on-flat Indentation			Loading-holding-unloading contact adhesion analysis	51,83-85
Flat punch Indentation				85-88

The peeling test is a commonly used testing geometry for the evaluation of adhesive toughness in terms of the average peel force normalized by the width. Specifically for hydrogels, it is most applicable where the gel may be peeled off a substrate—this is particularly relevant for hydrogels being used as adhesive patches<sup>80</sup>—or in similar cases to lap shear geometries, but where adhesive toughness is a concern.<sup>78</sup> In the peeling test the adhesive material is brought into contact with an adherend, after which one end is pulled away at an angle ( $\theta$ ) relative to the interface, at a finite speed. The two most commonly used values for  $\theta$  are  $90^\circ$  and  $180^\circ$ , depending on preference and the flexibility of the adhesive. Another geometry of peeling test is the T-peel test, where both adherends are pulled apart at one end as though each is undergoing  $90^\circ$  peeling. This geometry is particularly applicable when both adherends are thin and flexible.<sup>81,82</sup> The adhesive material can have a stiffer backing, which helps to prevent stretching of the sample during peeling.<sup>82</sup> The force required to peel the adhesive away from the bonded surface is measured as a function of peeling distance. The peeling force increases at the beginning to deform the adhesive materials until the strain energy is sufficient to overcome the bonding energy at the interface and reach a steady-state force plateau – the average peel force— where the adhesives are continually peeled away from the surface. Note that peeling involves the bending of the backing materials and deformation of the adhesives, resulting in significant influences from the mechanics and viscoelastic behavior of the adhesives on the peeling force. Nevertheless, the steady-state peeling force is typically recorded for characterizing adhesives. Since the value of the steady state peeling force is proportional to the width of the peeling front, the peeling force can be normalized by the width to report adhesion in units of N/m.

### 3.2 Analysis of adhesive contact behavior through indentation

Indentation is a technique that is better suited to investigating materials—including hydrogels—that are heterogeneous at the surface (i.e. consisting of more than one type of surface chemistry) or in the bulk of the material. In this technique a probe is brought into contact with a

substrate until a certain displacement or force is reached. After a prespecified holding time (which can range from no holding time to minutes or hours, depending on what is desired), the probe is withdrawn from the substrate until separation. A variety of information can be obtained from the indentation curve by examining both force versus distance and force versus time plotted during the loading-holding-unloading processes. The loading or approach step can provide information into the mechanical properties of the gel, such as the elastic modulus.<sup>87</sup> The unloading stage can give information about the adhesive behavior of the gel. The holding stage can provide insight into the relaxation behavior of the compressed gel, which is best observed when the force is plotted against time instead of distance, such as used by Arunbabu et al.<sup>84</sup> to investigate the effect of crosslinker density on relaxation of a hydrogel system. The difference between loading and unloading can provide information about hysteresis of the system, in which time-dependent physical or chemical interactions can cause the unloading behavior to be different. Of particular note is the pull-off force, which (as in tensile and lap shear adhesive tests) marks the highest adhesive force felt during detachment.

There are two typical geometries for indentation tests: (a) indenting a hemispherical (or curved) probe on a flat surface, and (b) indenting a flat punch on a flat surface. The hydrogels under investigation can be either the indenting material or the substrate surface, or both. The primary advantage of the flat punch geometry is that the contact area is constant and always known. This can be particularly useful for hydrogels, where similar refractive indices can make viewing the contact area difficult, particularly underwater.<sup>51</sup> Additionally, both sides of the test setup are flat sheets, allowing for easy formation of both the probe and substrate.<sup>86</sup> This is useful if a hydrogel is being used as a probe and is challenging to form into a sphere or hemisphere. However, proper alignment of the two planes is essential to ensure good contact and reliable measurements,<sup>85</sup> and there is a non-uniform stress distribution across the interface. In particular, high stresses are present at the edges of the contact between the punch and gel, resulting in increased strain and additional viscoelastic effects in this region.<sup>85,87,88</sup>

The probe-on-flat indentation geometry allows the variation of contact area with the compressive load. For many studies, a glass or silicone (polydimethylsiloxane, PDMS) probe is used and indented into the surface to be studied.<sup>83,84</sup> However, the gel itself can be formed into the probe and used to indent other materials; this can provide insight into the adhesive interactions between the hydrogel and a variety of other surfaces. Using the gel as a probe is particularly useful for investigating adhesion to materials that are difficult to form into other shapes, such as tissue.<sup>51</sup> The resulting indentation data can be interpreted in the framework of contact mechanics. The main forces responsible for adhesion are typically van der Waals forces. For two elastomeric materials in contact, the Johnson-Kendall-Roberts (JKR) technique has been widely used to relate the work of adhesion to the deformation (through the radius of contact,  $a$ ) and the load force ( $F$ ) through the equation:

$$a^3 = \frac{3R}{4E^*} \left( F + 3W_A \pi R + \sqrt{6W_A \pi R F + (3W_A \pi R)^2} \right) \quad (6)$$

where  $R$  is the radius of the probe tip and  $E^*$  is the reduced modulus of the system, related to the moduli of the probe and substrate through their Poisson's ratios ( $\nu$ ) by:

$$\frac{1}{E^*} = \frac{1 - \nu_1^2}{E_1} + \frac{1 - \nu_2^2}{E_2} \quad (7)$$

The pull-off force ( $F_c$ ) at the point of separation during the unloading process can be determined by the following equation.

$$F_c = -\frac{3}{2}W_A\pi R \quad (8)$$

When there is no adhesive interaction between the two materials ( $W_A = 0$ ), this equation becomes the Hertz equation, which was developed earlier and used to describe contact between non-adhesive elastic bodies:

$$a^3 = \frac{3FR}{4E^*} \quad (9)$$

or in its more common form:

$$F = \frac{4}{3}E^* R^{1/2} d^{3/2} \quad (10)$$

where  $d$  is the indentation depth, related to  $a$  by  $a = \sqrt{Rd}$ .

JKR theory is most commonly applied to dry surfaces in air. Although originally applied to materials like rubber, other reversible surface interactions can also be investigated with the JKR technique, which is important for hydrogels since it cannot rely on van der Waals forces in wet conditions. When used for hydrogel systems (whether in air or underwater), the presence of water means that only an effective work of adhesion can be obtained. In air, the water in the gel leads to additional forces such as capillary forces; underwater, the medium itself plays a role in the measured work of adhesion. Loskofsky et al.<sup>83</sup> showed that work of adhesion values based on surface energy could be obtained underwater, giving values only slightly smaller than those in air; however, the substrates they used were constrained to nonpolar materials to avoid complications from water interactions. Still, the effective work of adhesion that includes other interactions is a useful parameter for investigating the adhesive behavior of a hydrogel and its interactions with other materials.

#### 4 Bio-inspired adhesive strategy - catechol chemistry

To enhance the adhesion of hydrogel materials to wet surfaces, researchers have been looking into the chemistry of marine organisms, such as sandcastle worms and mytilus mussels, which are able to bind to diverse submerged substrates in a harsh and turbulent wet conditions.<sup>36,89</sup> Compared with adhesives under dry conditions, wet adhesives have several crucial requirements including breaking through surface bound water layers, being cohesive against water corruption, and programmed underwater curing. In 1981, Waite and Tanzer<sup>90</sup> identified a catecholic amino acid (DOPA) from the mussel foot plaque; and found it contributes significantly to the robust underwater adhesion of mussels. It has been revealed that the catechol-containing peptide was able to penetrate water boundary layers and form interfacial bonds with submerged substrates.<sup>90,91</sup>

In addition to the presence of DOPA amino acid, the catechol chemistry of bioadhesion involves a series of synergistic processes including *in vivo* coacervation and surface spreading/drying, followed by phase inversion triggered by environmental stimuli and covalent cross-linking in extended timescales.<sup>92</sup> Here we recapitulate the working mechanism of catechol from chemistry perspective and discuss the roles of catechol in contact adhesion of liquid proteins, coacervation of catechol-containing proteins/polymers, and curing for enhanced adhesive strength. It will provide guidelines for the further development of biomimetic design of catechol-functionalized adhesive hydrogels.

#### 4.1 Catechol chemistry in wet adhesives

Catechol groups feature a unique combination of hydroxyl groups and phenol groups; thus it can participate in various interfacial interactions such as hydrogen bonding, metal coordination,  $\pi$ - $\pi$ /cation- $\pi$  interactions, and thiol reduction.<sup>91</sup> These interactions provide instant and effective wet adhesion that can be further strengthened upon subsequent curing. Catechol groups undergo covalent cross-linking in oxidative conditions, which significantly improves the cohesive strength of wet adhesives for practical applications. In addition, it was recently found that catechol groups contribute to the formation of protein coacervate that is crucial for mussel adhesives.<sup>93,94</sup> Coacervate is a condensed and yet water immiscible fluid having excellent wettability on almost all water-submerged substrates. Electrostatic complexation, hydrogen bonding, and hydrophobic interactions have been recognized as important weak interactions driving polymer association and coacervation. Very recently, catechol group were found to promote coacervation through cation- $\pi$  interaction and hydrogen bonding.<sup>95-96</sup> These interactions work synergistically to promote instantaneous adhesion, polymeric coacervation, and curing adhesion (Figure 3).<sup>57,97</sup>

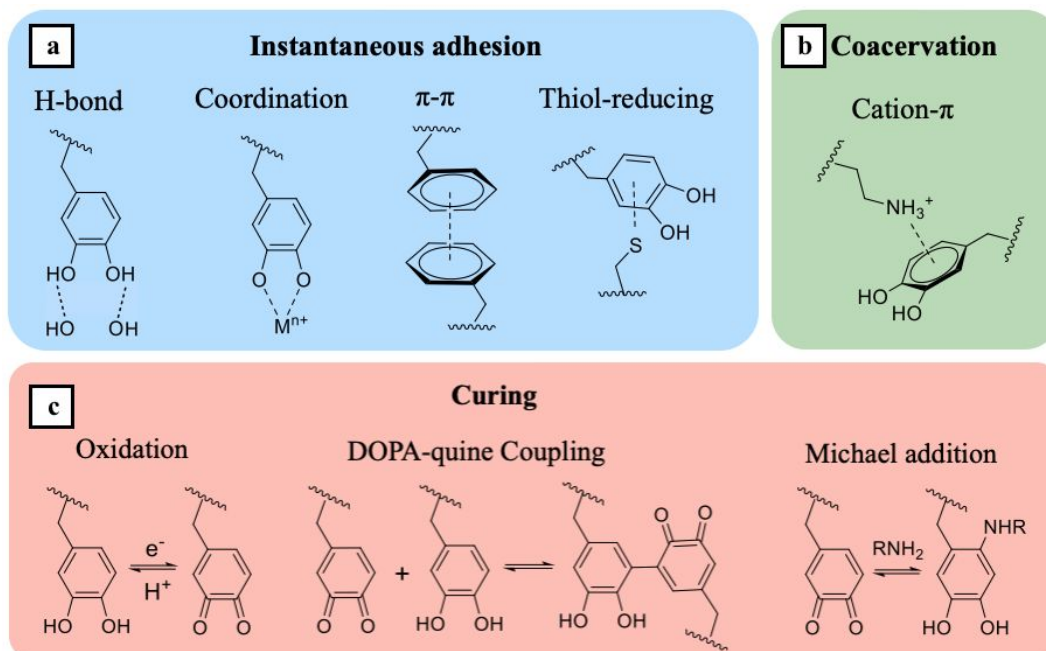


**Figure 3.** The multiple roles of catechol groups in wet adhesion: (a) instantaneous adhesion, (b) coacervation formation, and (c) wet adhesive curing.

## 4.2 Instantaneous adhesion

Instantaneous adhesion generally occurs as a result of the noncovalent interactions between wet adhesive materials and the targeted substrates. The binding energy of bidentate catecholic hydroxyls was demonstrated to induce hydrogen bonding with lifetimes that were orders of magnitude greater than that of the mono-dentate hydroxyl.<sup>98</sup> A single reduced DOPA residue exhibited strong, reversible adhesion to a wet metal oxide surface by non-covalent interaction (800pN).<sup>99</sup> However, the catecholic peptide is chemically unstable with increasing pH. Yu et al.<sup>100</sup> showed that the adhesion energy of mfp-3 (mfp-3) was enhanced at pH 3 on a mica surface. As the pH increased to 5.5, the adhesion decreased more than 4-fold. When the pH went up to 7.5, the quinone form dominated over catechol, accompanied by weakening of the hydrogen bond. Accordingly, mfp-3 adhesion was only 5% of that exhibited on mica at pH 3 (Figure 4b).<sup>100</sup>

Mfp-5 is another catechol-rich primer that enables surface adsorption, which shows maximum adhesion at pH 3, followed by a log decay with increasing pH.<sup>36</sup> Thus, to preserve the interfacial reactivity of non-oxidized catechol, mussels deliver adhesive proteins under acidic conditions (non-oxidized form) for strong interfacial binding, after which DOPA oxidation and curing occur gradually in seawater (pH 8).<sup>39,91,101-103</sup> In addition to pH regulation, mussels counteracts the formation of quinone by a cysteine-rich adhesive peptide mfp-6. The reactive thiols of mfp-6 can eliminate the O<sub>2</sub> content in the environment. The quinone-to-DOPA reaction can be induced by thiols, which revives the catechol-mediated hydrogen bonding and coordination. This strategy for reducing and preserving the adhesive form of catechol have been recently used to design synthetic mimics containing thiourea.<sup>104</sup>

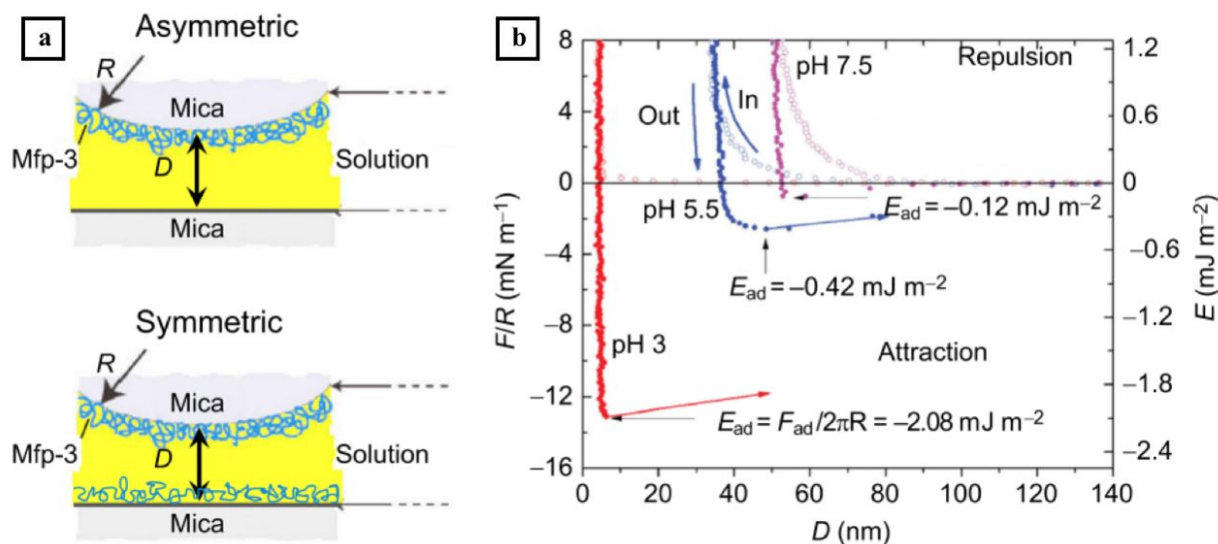


**Figure 4.** Effect of pH on molecular adhesion to the mica surface. (a) Asymmetric and symmetric tests of mussel foot proteins carried out using surface force apparatus (SFA). Asymmetric configuration is used to measure the interfacial adhesion, while the symmetric configuration tests the cohesion between protein monolayers (blue).  $D$ , distance;  $R$ , radius. Reproduced with permission from ref. 91. Copyright 2017 The Company of Biologists Ltd. (b) Asymmetric adhesion of mfp-3 at different pH values (3, 5.5, and 7.5). Reproduced with permission from ref. 100. Copyright 2011 Springer Nature Limited.



In addition to hydrogen bond, the conformation of the bidentate hydroxyls is susceptible to metallic materials through coordination bonds, derived from the interactions between phenol hydroxyls and metal atoms of the surface. The hydrogen bonding and coordination bonds usually coexist to maintain the interfacial bonding, both of which are highly pH dependent.<sup>100</sup> On the titanium oxide surface, as the pH is increased from 2 to 5, catechol transitions from hydrogen bonds to bidentate-binuclear coordinate bonds, and finally to two coordination bonds at pH  $\sim$ 8 (Figure 5A).<sup>105</sup> Though the coordination of catechol with other surfaces (e.g., Zn and Al) has been reported, it is noteworthy that DOPA coordination does not necessarily occur on all metallic surfaces.

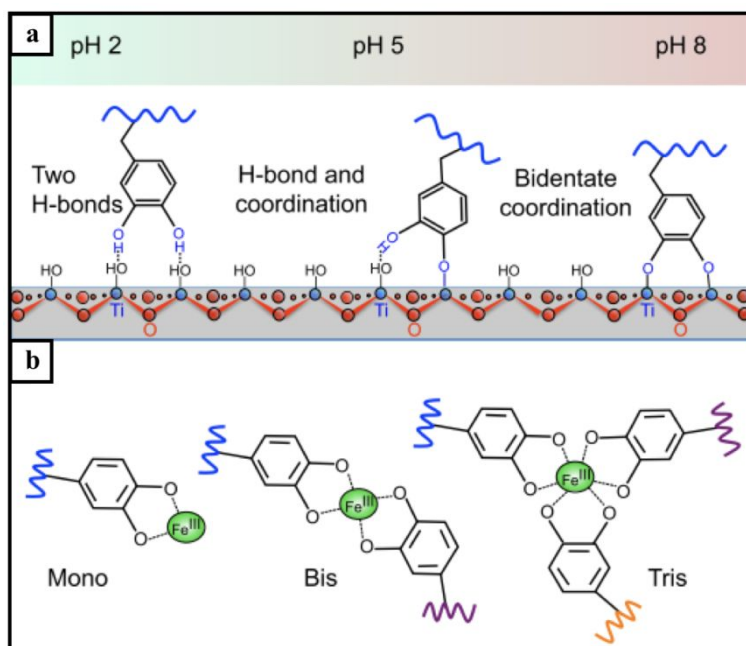


**Figure 5.** (a) pH-dependent transition from interfacial hydrogen bonding to coordinate bonds on the surfaces of metal oxide. (b) catechol-Fe<sup>3+</sup> stoichiometry varied from acidic pH  $\sim$ 2.0 to basic pH  $\sim$ 8.0. Reproduced with permission from ref. 91. Copyright 2017 The Company of Biologists Ltd.

Mussel byssus is rich in Fe<sup>3+</sup> due to catechol's ability to chelate metal ions by forming tris-catecholate-Fe<sup>3+</sup> complex.<sup>105</sup> When the pH shifted from acidic to weakly basic conditions (the pH of sea water is  $\sim$ 8.0), the iron-catechol stoichiometry changed from mono- to bis- and finally to the tris- (Figure. 5b).<sup>98</sup> In parallel with hydrogen bonding, this strong and reversible catechol-Fe<sup>3+</sup> coordination represents another important regulator for tuning mussel-derived catechol chemistry to achieve bulk cohesion, which is finally translated into robust adhesives.<sup>106</sup> Other metal ions such as Zn<sup>2+</sup>, Mg<sup>2+</sup>, Ca<sup>2+</sup>, Al<sup>3+</sup>, Cu<sup>2+</sup>, and boronate have also been reported to trigger the formation of metallosupramolecular polymers<sup>107,108</sup>

#### 4.3 Cation- $\pi$ interactions and coacervation

Coacervation is a liquid-liquid phase separation phenomenon that occurs as a result of the associative intermolecular interactions between different macromolecules upon aqueous mixing.<sup>109</sup> The formed coacervate is water immiscible and features low surface tension, rendering

it stable in disruptive water and spreadable on many submerged surfaces underwater.<sup>110</sup> It is an important method for marine organisms such as sandcastle worms and mussels to prepare bioadhesives. Given the abundance of charged macromolecules in biological systems and the facile synthesis of polyelectrolytes, complex coacervate has been widely exploited for the fabrication of wet adhesives both *in vivo* and *in vitro*.<sup>36,97</sup> Nevertheless, all of the more than 20 known mfps are cationic, with the anionic counterparts being absent,<sup>91</sup> indicating new interactions driving mfps coacervation in mussel systems.

Recently, the aromatic residue tyrosine (a precursor of the DOPA moiety) was reported to contribute to coacervation of mfp-1 via cation- $\pi$  interaction. Kim et al.<sup>95</sup> discovered the abundance and proximity of the tyrosine-lysine pattern from the protein sequence. To verify the possibility of cation- $\pi$  interaction for coacervation, a recombinant mfp-1 (rmfp-1) was designed, and mixed with a synthetic polyelectrolyte named poly(2-(trimethylamino)ethyl methacrylate) (MADQUAT)<sup>96</sup>. Interestingly, the mixing of positively charged rmfp-1 and MADQUAT in the presence of salt screening led to the occurring of coacervation at proper salt and polymer concentrations (Figure 6a). Through molecular force measurements and theoretical simulations, authors claimed that the coacervation is driven by the short-range cation- $\pi$  interaction by overcoming repulsive electrostatic interactions. In addition, single component coacervate of rmfp-1 driven by the lysine ~ tyrosine cation- $\pi$  interaction in the presence of a salt concentration ( $> 0.7$  M NaCl) close to seawater was further verified<sup>95</sup>. These discoveries are noteworthy for unraveling the puzzle that how coacervate form inside mussels when all mfps discovered so far are positively charged. It also points to new ways of engineering catechol-containing coacervates for advanced wet adhesives. For example, very recently Byeongseon et al. reported the coacervation of interfacial adhesive proteins (mfp-5) promoting initial adhesion to wet adhesive.<sup>111</sup> An alternative mechanism on basis of catechol involved cation- $\pi$  interaction was proposed by authors for coacervate formation and adhesive strength. It has also been pointed out the salt bridge interaction might also be plausible for the coacervate adhesive.

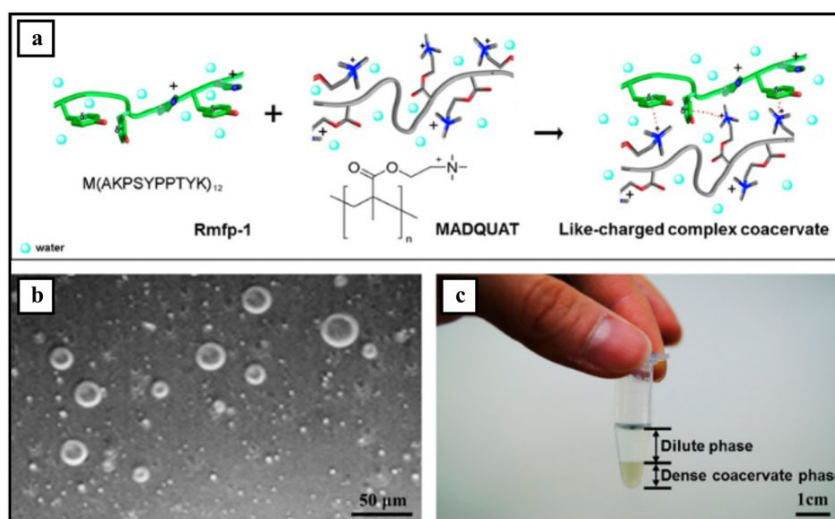


**Figure 6.** (a) Cation- $\pi$  interaction driven like-charge complex coacervate formation. (b) The obtained coacervate under light microscopy, and (c) its bulk phase separation. Reproduced with permission from ref. 96. Copyright 2016 National Academy of Sciences.

The energetics of the cation- $\pi$  bonds were further investigated by surface force apparatus using lysine-rich peptides as the model molecules. It was revealed that all three aromatic residues (Phe, DOPA, and Tyr) induced cation- $\pi$  interaction with lysine, and the cohesiveness of this interaction was able to compete with those of the strong intermolecular interactions of mussel adhesive proteins.<sup>112</sup> The importance of catechol-cation synergy has also been reported to enhance interfacial interaction. Maier et al.<sup>57</sup> investigated catechol-containing siderophores from the plant pathogen *Dickeya chrysanthemi*, and observed the adjacent catechol-lysine placement in the chemical structure, demonstrating their synergistic interplay in underwater adhesion.<sup>57,113</sup> The lysine residue was able to evict hydrated cations at the mica surface easing the catechol binding. In addition, the catechol was oxidation-resistant as the siderophores exhibited robust adhesion energy from pH 3.5 to pH 7.5.<sup>57</sup>

Catechol-derivatives are also able to facilitate coacervate formation through hydrogen bonding. Shin et al.<sup>114</sup> reported that intermolecular hydrogen bonding between tannic acid (TA) and poly(ethylene glycol) (PEG) drives the formation of ready-to-use coacervate and wet adhesive for biomedical purpose. Adhesion strength of the coacervate could be tuned by varying the numbers of PEG arms and end-group moieties (-NH<sub>2</sub>, -OH, and -SH), and it was applied as a biodegradable patch for in-vivo detection of gastroesophageal reflux diseases.<sup>114</sup> Owing to its long-lasting esophageal retention time, TA-PEG adhesive is promising as a mucoadhesive material.<sup>115</sup> This recent progress has enhanced our understanding of catechol chemistry and laid a strong chemical foundation for the future development of catechol-involved coacervate and wet adhesives.

#### 4.4 Curing for strength development

Despite the importance of non-oxidized catechol for interfacial interactions, delicate control of catechol oxidation is of equal importance to the strong adhesion and cohesive strength of mussel plaques. In 1999, Waite and co-workers<sup>116</sup> discovered the formation of quinone-derived cross-linking in the mussel byssus. Although the occurrence of such covalent cross-links is limited, it contributed significantly to the cohesion of the cured protein adhesives. Rate and extent of curing can be tuned by reaction pH, time, as well as the presence of oxidants. Additionally, catechol cross-linking plays an active role in the formation of the porous microstructures found in mussel plaques, thus enabling dissipation of fracture energy.<sup>39</sup>

Catechol oxidizes to form the highly reactive quinone, which can participate in covalent cross-linking (Figure 7). In the presence of chemical stimuli, such as elevated pH (pH above 5.5), polyphenol oxidase, metal ions or some oxidizing agents (NaIO<sub>4</sub> etc.), the catechol dimerizes and subsequently polymerize resulting in the curing of catechol containing adhesive).<sup>117,118</sup> Increased cross-linking can increase the bulk strength of wet adhesives.<sup>97</sup> A weakly basic condition (at pH values of ~8–8.5) can also induce progressive cross-linking to enhance cohesion of catechol-containing adhesive.<sup>119,120</sup> Other functional groups such as -NH<sub>2</sub> and -SH can react with quinone via Michael addition, which was widely confirmed for both mfps and their synthetic analogues.<sup>121</sup>

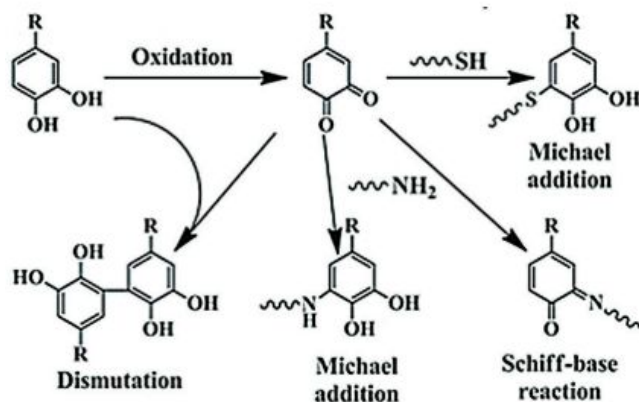


**Figure 7.** Oxidative cross-linking pathways for catechol-containing molecules. R group represents the backbone of the polymer. Reproduced with permission from ref. 98. Copyright 2019 Wiley-VCH.

Catechols that contain a free amine group (i.e., dopamine) undergo intra-molecular cyclization between the catechol side chain and the amine group to form a leukochrome that can undergo polymerization similar to melanin formation.<sup>118</sup> The use of polydopamine (PDA) as an adhesive primer and grafting of multifunctional polymers through a simple dip-coating process in an aqueous medium was reported in 2007 (Figure 8).<sup>42</sup> Thus far, the use of PDA has become a facile and robust approach in designing multifunctional materials.<sup>122-125</sup> In recent years, PDA has also found use in the preparation of adhesive hydrogels that can potentially be used as soft electronics, biomimetic skins, and tissue adhesives.<sup>126-129</sup>

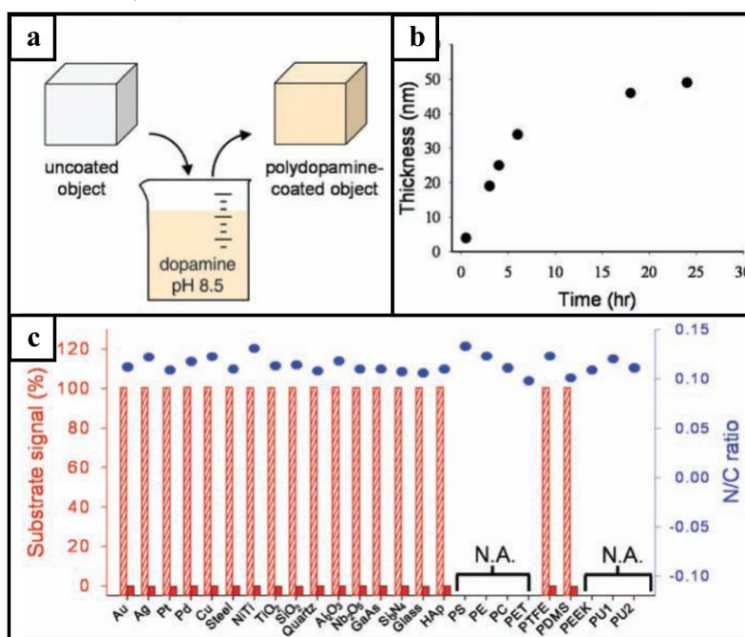


**Figure 8.** (A) Schematic representation of the dip-coating of an object in dopamine solution at pH 8.5. (B) Thickness evolution of the formed polydopamine films. (C) XPS characterization of 25 polydopamine-coated surfaces. The bar graph represents the intensity of the characteristic substrate signal before (hatched) and after (solid) coating with polydopamine. Reproduced with permission from ref. 42. Copyright 2007 Macmillan Publishers Limited.

## 5. Catechol-functionalized adhesive hydrogels

The representative examples of mussel wet adhesives discussed in section 4 have demonstrated the special natures of both permanent and temporary underwater attachments.<sup>130–133</sup> There have been extensive research effort on the characterization of mussels so as to exploit them as a popular inspiration for biomimetic wet adhesives.<sup>35,134,135,136</sup> This section review the recent progress of using catechol moieties of DOPA to engineer adhesive hydrogels.

Early examples of catechol-containing adhesive systems include polypeptide-based copolymers prepared by Deming and co-workers,<sup>137</sup> and styrene-based copolymers prepared by Wilker and co-workers,<sup>138</sup> which showed exceptionally high adhesion strengths to various surfaces in wet conditions when equipped with catechol functional groups (Figure 9a and 9b). Inspired by this pioneering work, many catechol-based adhesive hydrogels have been fabricated from catechol-containing polymers such as protein- and peptide-based versions of the mfps, catechol-functionalized monomers, and synthetic DOPA-containing polymers (Figure 9c).<sup>139–143</sup> Catechol moieties are able to polymerize in the hydrogel network to form covalent bonds and noncovalent bonds with the matrices, which contribute to the cross-linking process to form a gel network.<sup>142</sup> However, they are believed to suffer from oxidation. Alternative gelation mechanisms involving temperature or UV induced cross-linking of catechol-functionalized polymers have been proposed instead of relying on oxidizing agents, however catechol moieties are generally reactive and tend to lose adhesion properties when interacting with other functional groups.<sup>24</sup> Therefore, specifically designed catechol-containing copolymers are formulated and physically assembled to form cross-linked hydrogels where the catechol groups are carefully protected from oxidation. This section will review the synthetic approaches of catechol-based adhesive hydrogels, and the effects of interfacial properties and nanostructure to their adhesive performance.

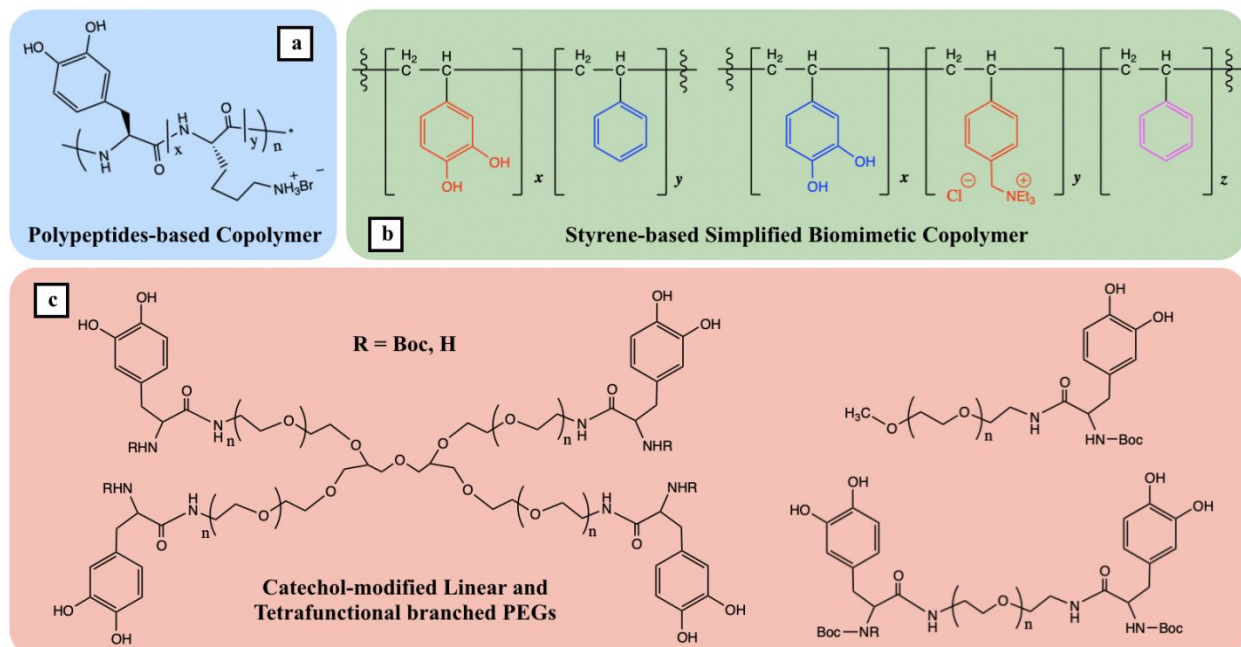


**Figure 9.** Chemical structures of (a) N-carboxyanhydride co-polypeptides, (b) styrene-based copolymers, (c) DOPA-modified PEGs with four different ligands.

## 5.1 Synthetic approaches

There have been many efforts to develop underwater adhesive hydrogels by incorporating catechols into synthetic polymers. Below, we present a few illustrative examples of catechol-functionalized adhesive hydrogels and categorize their fabrication methods into three synthetic approaches (Figure 10), which will hopefully provide a rational guideline for designing functional hydrogels with adhesive properties.

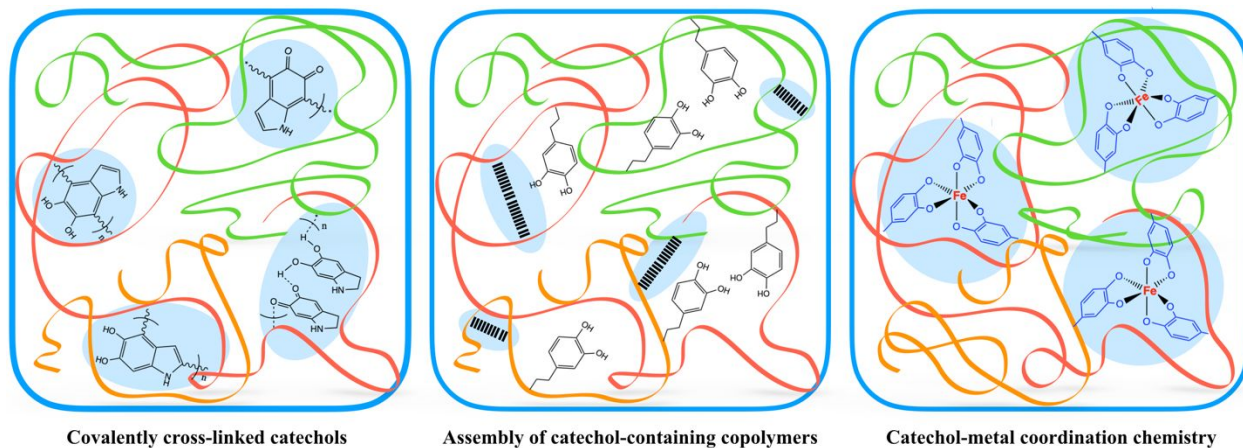


**Figure 10.** Synthetic approaches for the preparation of catechol-functionalized adhesive hydrogels through (a) catechol cross-linking, (b) assembly or cross-linking of catechol-containing copolymers, and (c) catechol-metal coordination chemistry.

### 5.1.1 Covalently cross-linked catechols

Catechols are easily oxidized to quinones, leading to the cross-linking of catechol-bearing molecules and contributes to the gelation process. Catechol end-capped PEG has been widely investigated as the structural polymer in the preparation of adhesive hydrogels, with the chemically inert PEG segment being chosen to provide the integrity of the 3D network (Figure 9c). This system was originally designed by Messersmith and co-workers,<sup>148</sup> who prepared both linear and tetrafunctional branched PEG platforms decorated with catechol that serves to promote both interfacial and cohesive cross-linking. Owing to the hydrophilic nature of both the PEG and catechol groups, these water-soluble polymers were easily cross-linked into hydrogels upon chemical or enzymatic oxidation by  $\text{NaIO}_4$ , horseradish peroxidase- $\text{H}_2\text{O}_2$ , or mushroom tyrosinase- $\text{O}_2$ .<sup>144–148</sup> The gelation time of these biomimetic hydrogels was highly dependent on the structure and molecular weight of the PEG, as well as the type and concentration of the oxidizing reagents.

Using a similar strategy, Park and co-workers<sup>147</sup> formulated an injectable hydrogel based on the covalent cross-linking of hyaluronic acid and a Pluronic polymer. As illustrated in Figure 11a and 11b, catechol and cysteamine groups were first conjugated to the backbone of hyaluronic acid and the end group of Pluronic F-127, respectively, then the two functionalized polymer solutions were homogeneously mixed and became a cross-linked adhesive hydrogel. In this design, inter- and intramolecular cross-linking was achieved between the oxidized catechol groups and the thiol groups via Michael addition. The same research group extended this system to catechol-

grafted chitosan and thiol-capped Pluronic polymers, which were cross-linked via catechol-thiol reactions (Figure 11c).<sup>148</sup> Both precursors were soluble and premixed at 4°C, the resulting viscous solution instantly solidified into a gel state when the temperature was increased to 37°C. Pluronic polymer was introduced to realize temperature-responsive sol–gel transition and tune the gelation speeds for injectable applications.

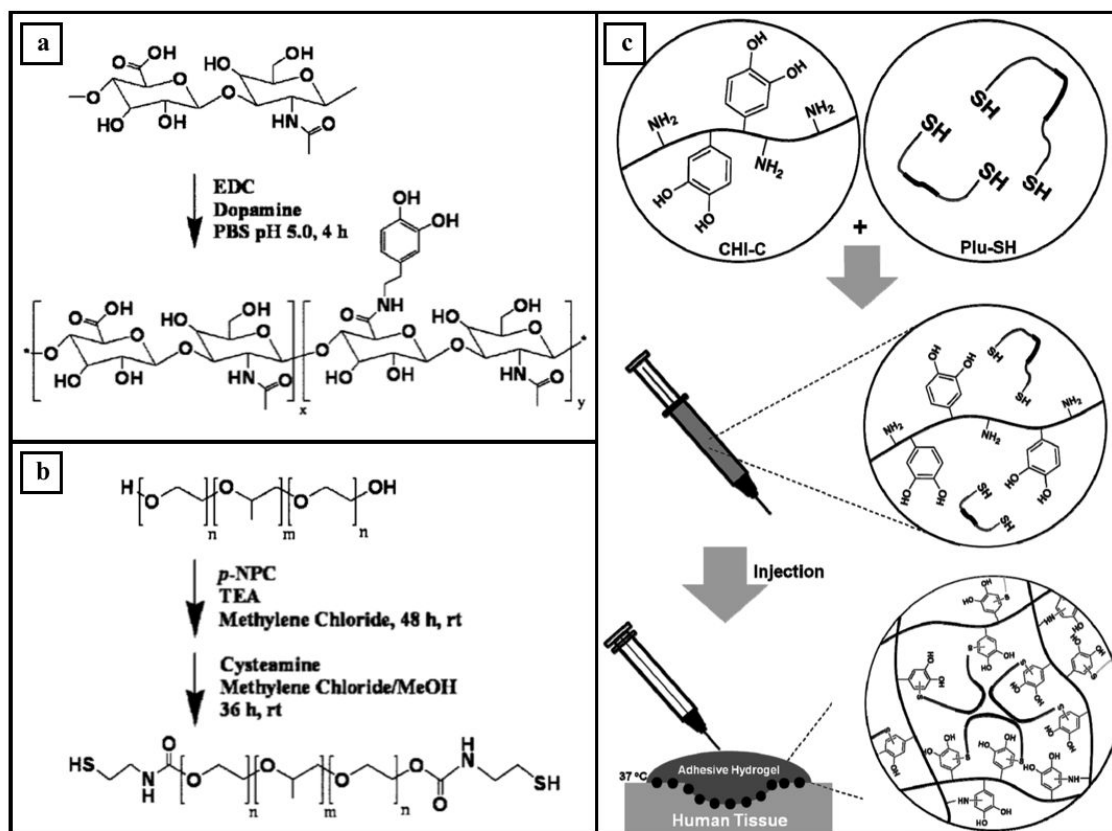


**Figure 11.** The synthesis and chemical structure of (a) catechol-conjugated hyaluronic acid and (b) cysteamine-conjugated Pluronic F-127. Reproduced with permission from ref. 147. Copyright 2010 The Royal Society of Chemistry. (c) In situ preparation of cross-linkable CHI-C/Plu-SH hydrogels. Reproduced with permission from ref. 148. Copyright 2011 American Chemical Society.

### 5.1.2 Assembly and cross-linking of catechol-containing copolymers

Cross-linking through catechol moiety makes use of the oxidative polymerization process of catechol, which is a simple approach for forming cross-linked hydrogels in-situ. However, the key to achieving strong adhesion is to control the degree of oxidation and maintain a high concentration of catechol in its reduced form. Messersmith and co-workers<sup>149</sup> conjugated catechol moieties to Pluronic-based block copolymers (Figure 12a), which were soluble in water and aggregated into micelle hydrogels at a certain temperature depending on their composition and concentration. To prevent the catechol groups from oxidizing during the coupling reactions, sodium borate was introduced to form borate-protected catechols, which were subsequently de-protected under acidic conditions. Similarly, Shull and co-workers<sup>150</sup> grafted catechol moieties to the center-block of poly(methyl methacrylate)-poly(methacrylic acid)-poly(methyl methacrylate)

(PMMA-PMMA-PMMA) (Figure 12b). This ABA triblock copolymer forms a physically cross-linked hydrogel through the self-assembly of the terminal hydrophobic end-blocks when exposed to water (Figure 12c). These approaches take advantage of the ability for the polymer to form a physically cross-linked network without using the oxidative cross-linking of catechol and preserves catechol in its unoxidized form for strong interfacial binding.

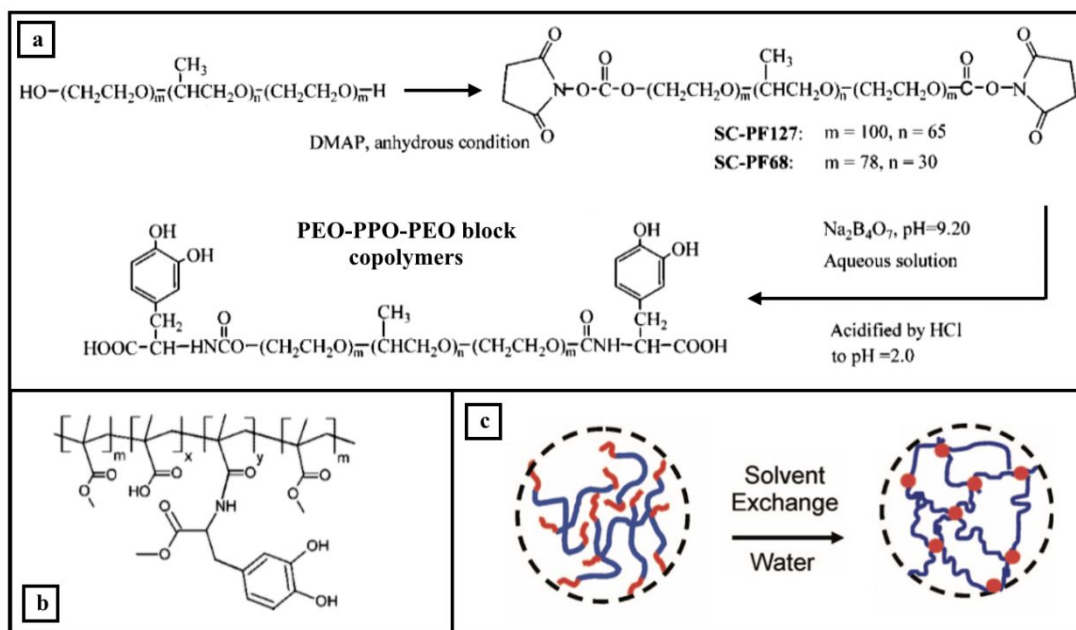


**Figure 12.** (a) Synthetic pathways for DOPA-modified Pluronic block copolymers. Reproduced with permission from ref. 149. Copyright 2002 American Chemical Society. (b) Chemical structure of DOPA-modified methacrylic triblock copolymer and (c) its self-assembly into hydrogel when exposed to saturated water. Reproduced with permission from ref. 150. Copyright 2008 American Chemical Society.

An ABA triblock copolymer consisted of a central hydrophilic poly(ethylene glycol) (PEG, “B” block) flanked by hydrophobic poly(lactic acid) (PLA, “A” block) was created, which was further modified with methacrylate group at the end of the “A” block and the adhesive DOPA-containing peptide in the middle of the “B” block (Figure 13a).<sup>151</sup> When dissolved in a solution, the triblock copolymer cured within few seconds through photo-initiated polymerization, due to the high effective concentration of the methacrylate groups accumulating in the hydrophobic domains and phase separated from the radical quenching catechol. This hydrogel demonstrated  $W_A$  values as high as  $410 \text{ mJ/m}^2$  to Ti surface. Another method to perform free-radical polymerization in the presence of catechol is to remove molecular oxygen from the precursor solution. Chung et al.<sup>152</sup> first demonstrated this by copolymerizing dopamine methacrylamide (DMA) with 2-methoxyethyl acrylate (MEA) to form a linear polymer, which were subsequently employed by others to form a network using a bifunctional cross-linker (Figure 13b). Similarly, a series of thermo-responsive copolymers composed of an adhesive block, a hydrophilic block, and a cross-linking block were synthesized via fragmentation chain transfer polymerization (Figure 13c).<sup>153</sup> These highly branched copolymers gelled efficiently when combined with photo-initiators,



which were used to cross-link the acrylate or methacrylate chain-ends while preserving the non-oxidized form of the catechols.

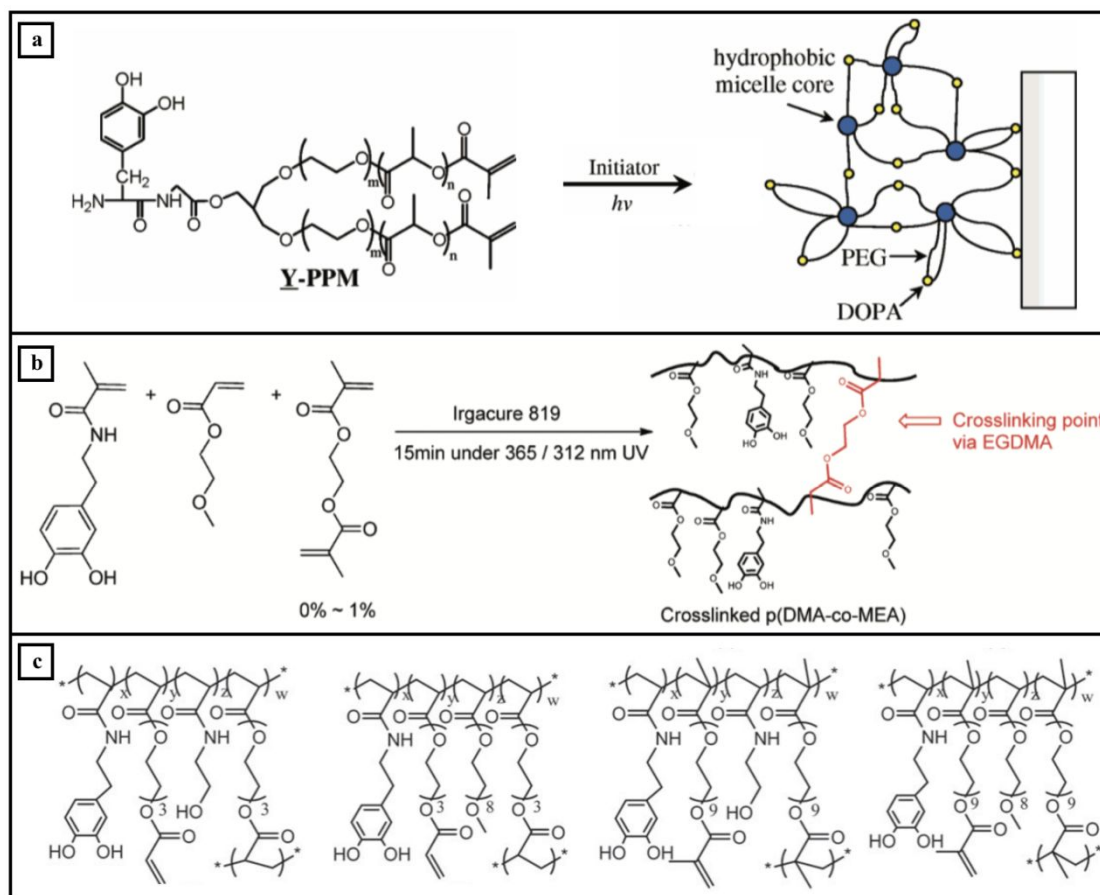


**Figure 13.** (a) Photopolymerization of DOPA-modified triblock copolymer consisted of a PEG mid-block and PLA end-blocks. Concentrating the polymerizable methacrylate groups in the hydrophobic micelle core promoted rapid photo-initiated polymerization. Reproduced with permission from ref. 151. Copyright 2006 American Chemical Society. (b) Photo-initiated polymerization of cross-linked poly(DMA-co-MEA). Reproduced with permission from ref. 152. Copyright 2011 American Chemical Society. (c) Chemical structures of highly branched PEG-catechol copolymers. Reproduced with permission from ref. 153. Copyright 2015 Wiley-VCH.

### 5.1.3 Catechol-metal coordination chemistry

To create hydrogels using catechol-metal ion coordination chemistry, Holten-Andersen et al.<sup>154</sup> combined 4-armed catechol-modified PEG cross-linked via catechol- $\text{Fe}^{3+}$  coordination. At a basic pH, formation of bis- and tris-catechol- $\text{Fe}^{3+}$  complexes promoted the formation a synthetic polymer network (Figure 14a). They further expanded the metal ions to  $\text{V}^{3+}$  and  $\text{Al}^{3+}$ , demonstrating that catechol-metal coordination bonds could be applied as a strong driving force for the cross-linking of these hydrogels (Figure 14b).<sup>155</sup> Using a similar strategy in which catechol moieties provide anchoring points for metal ions, Campo and co-workers<sup>156</sup> prepared hydrogels by combining PEG-functionalized with nitrodopamine with  $\text{Fe}^{3+}$  (Figure 14c). The linkage connecting nitrodopamine to PEG is photo-cleavable and the metal ion cross-linked hydrogel degraded via light irradiation. In addition to metal ions, Messersmith and co-workers<sup>108</sup> reportedly

used a bifunctional phenylboronic acid, 1,3-benzenediboronic acid, to function as a pH-responsive cross-linker with catechol-functionalized PEG (Figure 14d). Under alkaline conditions, formation of catechol-boronate complex resulted in the curing of the PEG hydrogel. This complex is reversible and dissociated at acidic pH. These metal ion and boronic acid-mediated complexation are reversible in nature and these hydrogels exhibit self-healing properties through the breakage and reformation of the coordination bonds.

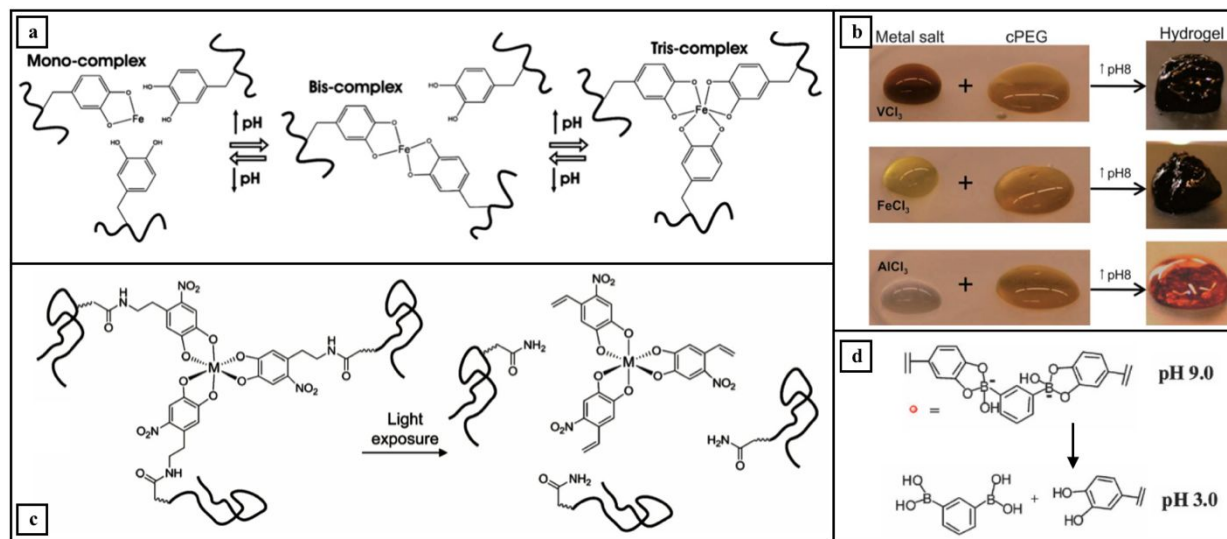


**Figure 14.** (a) Catechol forms pH dependent mono-, bis-, and tris-DOPA- $\text{Fe}^{3+}$  complexes with increasing pH. Complexation associated with elevated stoichiometry resulted in the formation of hydrogel. Reproduced with permission from ref. 154. Copyright 2011 National Academy of Sciences. (b) Photographs of the precursor solutions (left) and cross-linked hydrogels (right) formed by mixing three trivalent metal ion ( $\text{V}^{3+}$ ,  $\text{Fe}^{3+}$ ,  $\text{Al}^{3+}$ ) with PEG-catechol. Reproduced with permission from ref. 155. Copyright 2014 The Royal Society of Chemistry. (c) Photo-initiated degradation of nitrodopamine-PEG hydrogel cross-linked with metal ion. Reproduced with permission from ref. 156. Copyright 2012 Wiley-VCH. (d) pH-responsive hydrogel based on the interaction of PEG-catechol with 1,3-benzenediboronic acid through the formation of catechol-boronate complexation. Reproduced with permission from ref. 108. Copyright 2011 The Royal Society of Chemistry.

## 5.2 Hydrogel interfaces and nanostructures

Hydrogels with substantially improved adhesive properties have been achieved by engineering their interfaces and nanostructures. Most hydrogels—including catechol-functionalized hydrogels—are porous, which provides a high surface area that facilitates strong interaction between the catechol groups and the substrates. Nevertheless, their hydrophilic nature makes it difficult to displace water from the adhesive interface and water can weaken many forms of chemical bond. Therefore, the development of more compatible, effective, and stable interfaces has been one of the most interesting challenges for adhesive hydrogels. Zhao and co-workers<sup>157</sup> developed an adhesive hydrogel utilizing sequential delivery of components to localize adhesive dopamine directly at the interface and combine it with alginate for bulk cohesion. As demonstrated in Figure 15, a precursor solution of dopamine and  $\text{Fe}^{3+}$  is first applied to the surface, immediately followed by alginate.  $\text{Fe}^{3+}$  coordination and dopamine polymerization cross-link the hydrogel and link together adhesive and cohesive components. This sequential delivery approach promotes adhesion at the interface and greatly improves the underwater adhesion properties of the hydrogel.

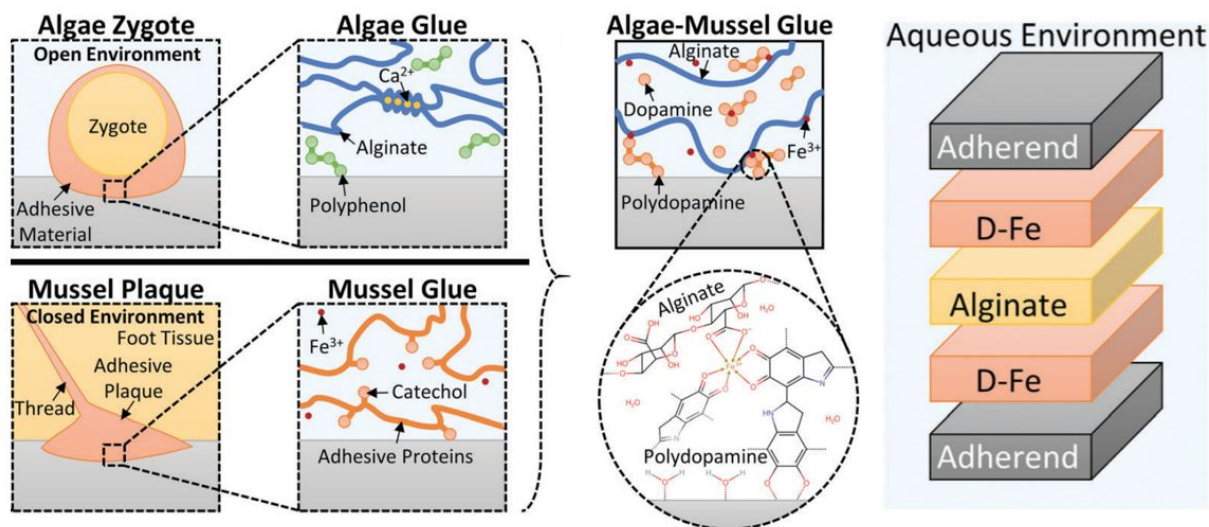


**Figure 15.** Illustration of a mussel-inspired hydrogel adhesive: surface functionalization of the substrates immobilizes dopamine, which forms coordinate bonds with the ferric ions and alginate solution is injected in between to provide bulk cohesion. Adapted with permission from ref. 157. Copyright 2019 Elsevier.

In addition to controlling the interfacial properties at the molecular level, the hydrogel and substrate interface can be rationally designed by introducing a patterned architecture. Messersmith and co-workers<sup>43</sup> coated p(DMA-co-MEA) onto an array of gecko-mimetic nanoscale pillars, which can be prepared with different dimensions and spacings (Figure 16a). This hybrid biomimetic adhesive demonstrated almost 15-fold increase in adhesive properties in the presence of moisture while maintaining its adhesive performance for over 1000 contact cycles in both dry and wet environments. The performance of the adhesive could be further enhanced through tuning the geometry of the nano-structures<sup>158</sup> as well as chemical cross-linking of the p(DMA-co-MEA) coating.<sup>159,160</sup> Recently, a stimuli-responsive adhesive hydrogel consisting of DMA and phenylboronic acid was chemically linked to an array of PDMS micropillars.<sup>161</sup> This pH responsive adhesive demonstrated strong wet adhesion at pH 3 ( $W_A = 420 \text{ mJ/m}^2$ ) and an reduction in adhesion value by 1-2 orders of magnitude at an elevated pH, as a result of catechol-boronate complexation. The adhesive can be repeatedly deactivated and reactivated by changing the pH. Most importantly, the micropillar structure increased the surface-to-volume ratio of the coated hydrogel and enhanced the rate of diffusion of ions needed to change the pH within the adhesive network. The hydrogel coated pillars demonstrated significantly faster rate of transition (1 min) between its adhesive and non-adhesive states, when compared to a bulk hydrogel (30-60 min).<sup>162</sup>

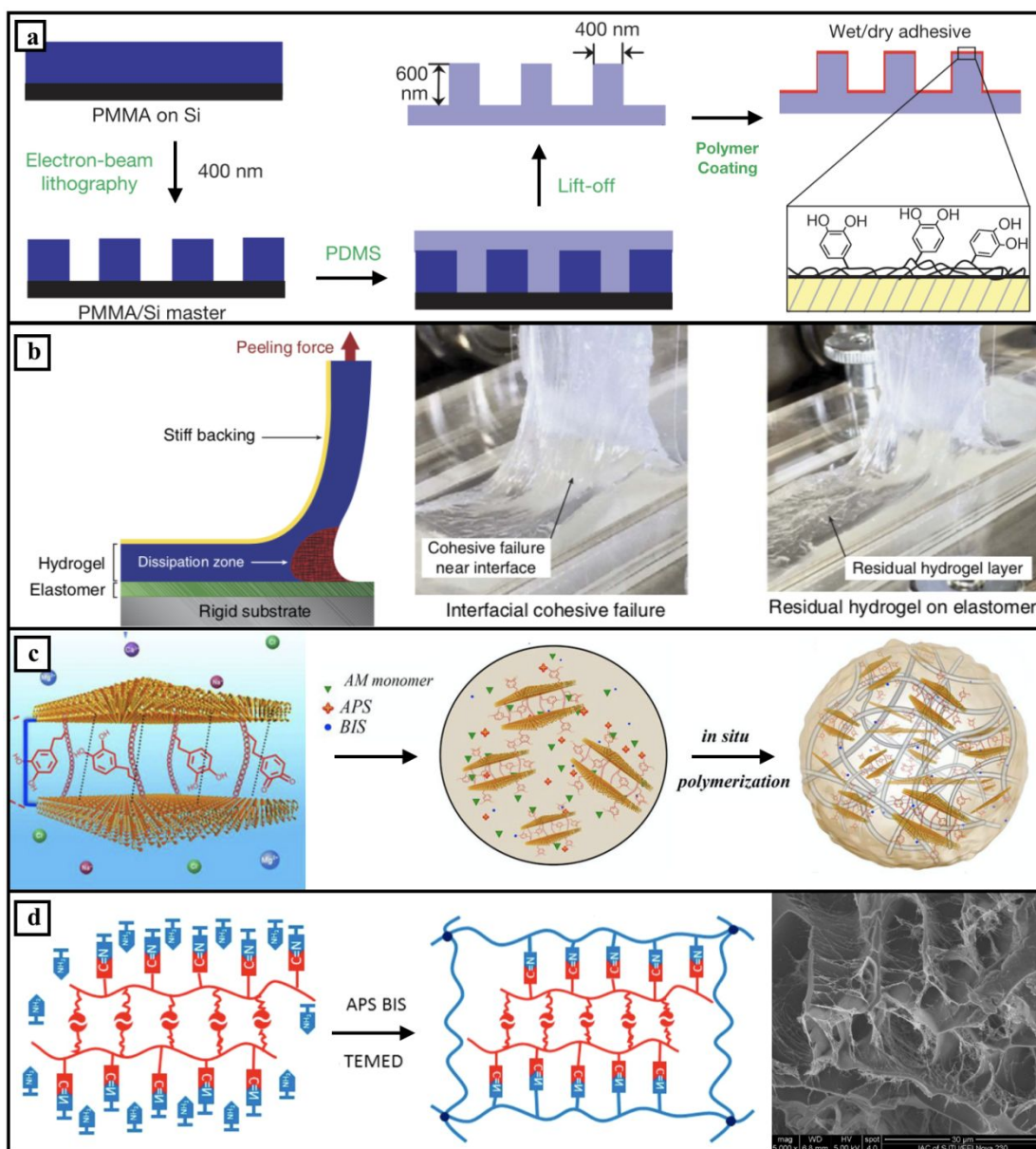


**Figure 16.** (a) Fabrication of p(DMA-coMEA)-coated nanopillar using electron-beam lithography. Adapted with permission from ref. 43. Copyright 2007 Springer Nature Limited. (b) Strong hydrogel-elastomer interaction induces a cohesive failure near the interface during the peeling test. Adapted with permission from ref. 163. Copyright 2016 Springer Nature Limited. (c) The formation of PDA-clay-PAM hydrogel via in situ polymerization. Adapted with permission from ref. 23. Copyright 2017 American Chemical Society. (d) The design mechanism for a double-network adhesive hydrogel and the interconnected microfibrils in the 3D nanostructure. Adapted with permission from ref. 164. Copyright 2018 American Chemical Society.

The integration of hydrogels with target applications requires not only strengthening the interactions between the two surfaces, but there is also a need to integrate an energy dissipative hydrogel matrix with high toughness and stretchability to provide strong cohesion. As recently demonstrated by Yuk et al.,<sup>163</sup> when hydrogel-elastomer interactions are sufficiently strong, a cohesive failure may occur near the interface during the peeling test (Figure 16b). Therefore, in

addition to focusing on the interfacial bonding mechanism of the hydrogels, their mechanical properties are equally important for the overall adhesion performance. Lu and co-workers<sup>23</sup> designed an adhesive polydopamine-clay-polyacrylamide hydrogel, in which PDA provided a high concentration of catechol groups and intercalated clay sheets acted as nano-reinforcement fillers. These adhesive hydrogels also exhibited excellent stretchability and toughness due to the presence of uniformly dispersed lamellar clay that was interwoven into the well-connected nanostructures (Figure 16c). The instant adhesion strength was above 30 kPa on human skin, and can be easily peeled from the skin without causing harm, allergic reaction, or leaving residue. To improve the mechanical properties of adhesive hydrogels, Liu et al.<sup>164</sup> utilize the concept of the tough double-network hydrogel to combining two polymer networks consisting of physically cross-linked catechol-grafted oxidized sodium alginate and chemically cross-linked PAM network to formulate an adhesive hydrogel (tensile strength up to 0.109 MPa and stretchability up to 2550%). The SEM image in Figure 16d confirmed the existence of the interconnected microfibrils in the 3D nanostructure, which are responsible for the superior tensile strength and stretchability of the adhesive hydrogel.

## 6. Biomedical applications of catechol-functionalized hydrogels

Natural and synthetic polymer hydrogels are functionalized with catechol moieties to develop adhesive hydrogels for different biomedical applications. These biomaterials are designed using the unique reduction-oxidation (redox) chemistry of catechol and its ability to form responsive and reversible interactions. In this section, we review catechol-based adhesive hydrogels designed for tissue repair and regeneration, antifouling and antimicrobial applications, drug delivery, and cell encapsulation and delivery (Table 2).

**Table 2:** Applications of catechol containing hydrogels.

Application	Composition	Description	Ref
Hemostasis	Chitosan-Pluronic	Gel rapidly after blood contact reducing bleeding in rat liver model	148
	Chitosan-ethylene glycol	Gel rapidly after blood contact with a reduced immune response	165
	Partially oxidized chitosan	Thin film coating which hydrate and gel rapidly after blood contact forming a hydrogel plug with elastic modulus of 93 kPa	166
Dermal Membrane Repair	PAM	Enhanced wound closure in rat with minimized scar tissue formation	142
	OSA-PAM	Self-healable interpenetrated hydrogel with enhanced cellular infiltration	164
Fetal Membrane Repair	PEG	Nontoxic hydrophilic hydrogel prevents cellular infiltration	167
		Burst strength of 50 kPa on fetal membrane	168

Myocardium Repair	Hyperbranched polyaminoester	Electro conductive hydrogel reducing infarction area 90.8 kPa adhesion strength on porcine myocardium	169
Hepatic Tissue Repair	PEG-EPL	Reduced bleeding in rat bleeding liver with 150 kPa adhesion strength	170
Antifouling and Antimicrobial	DNODN	Triblock thermoresponsive hydrogel preventing adhesion Caco-2 cells	171
	Catechol-PEG (A)-PMETA(B)	ABA hydrogel with cationic side chain preventing adhesion Caco-2 cells	172
	Citrate-PEG	Carboxyl groups suppressed both <i>S. aureus</i> and <i>E. coli</i>	173
	Zwitterionic sulfobetaine	Bacteriostatic against <i>E. coli</i> , <i>S. aureus</i> , and <i>Pseudomonas aeruginosa</i>	174
	HEAA microgels	Release superoxide and H <sub>2</sub> O <sub>2</sub> which prevents colony formation on <i>E. coli</i> and <i>Staphylococcus epidermidis</i> and reduced infectivity of both bovine viral diarrhea virus and porcine parvovirus	175
	Cl-DOPA-PEG	Prevent adhesion of <i>E. coli</i> by up to 90%	176
	Tannin	Silver nano particle loaded killing <i>S. aureus</i> , <i>E. coli</i> , and <i>C. Albicans</i>	177
Drug Carriers	Chitosan	pH-responsive mucoadhesive drug carrier for treatment of inflammatory bowel disease and cancer	178-180
	HA/Pluronic	Thermo-responsive injectable mucoadhesive drug carrier with adhesion strength of 7kPa in vitro	147
	Alginate	Strong injectable mucoadhesive drug carrier for the treatment of vulnerable atherosclerotic plaques	181
	PDA nanoparticles - encapsulated hydrogel	Catechol-boronate complexation-based drug release for cancer therapy via BTZ-loaded PDA nanoparticles	182
	P(AA-co-4-VPBA) nanogel- (Poly(DMA-co-PEGMA)) hydrogel	Catechol-boronate complexation-based drug release for cancer therapy via DOX-loaded phenylboronic acid nanogels	183
	PDA capsule w/wo PGA	Degradation-based drug release, PGA promoted degradation	184-185
	PMAA-PDA capsule	pH-responsive drug release for cancer therapy via DOX-tethered PMAA	186
	HA-PEG-MPN capsule	pH-responsive drug release with targeted delivery for cancer therapy	187
Cell Encapsulation and Delivery	Alginate	hNSCs /HUVECs encapsulation with no cytotoxicity and inflammatory responses	188
	PEG	Islet cells transplantation, fast normoglycemic recovery after 100 days	146

---

HA	hNSCs/ hHEPs/ hADSCs encapsulation, enhanced angiogenesis and osteogenesis, improved hepatic function	189-191
----	---	---------

---

## 6.1 Tissue sealant and adhesive

Damaged tissue with an open wound results in fluid leakage and has a diminished ability to act as a barrier to prevent infection.<sup>192,193</sup> A bioadhesive hydrogel designed for wound closure needs to have suitable adhesive properties, bulk cohesive properties, biocompatibility, and biodegradability to promote rapid tissue healing and regeneration.<sup>192–195</sup> However, different types of tissue and injury have different requirements, and it is necessary to design an adhesive specific to the desired application.<sup>139,196,197</sup> Here, adhesive hydrogels designed for hemostatic application and the repair of dermal tissue, fetal membrane, myocardial tissue, and hepatic tissue are summarized in Figure 17 and discussed below.

### 6.1.1 Hemostatic agents

A hemostatic system is a complex coordinated interaction between vasculature, platelets, cells, and plasma-borne coagulation factors, to maintain a balanced hemostatic state and prevent blood loss.<sup>194,198</sup> Delayed hemostasis can arise as a result of abnormalities in one or more of these components, which can cause fear, discomfort, and uncontrolled bleeding.<sup>166,199,200</sup> Chitosan has attracted considerable attention for hemostatic applications owing to its biocompatibility, biodegradability, and hemostatic activity through effective induction of platelet aggregation and adhesion at the injury site.<sup>165,201,202</sup> Therefore, various versions of catechol-functionalized chitosan have been reported as hemostatic agents.

A thermo-responsive adhesive consisting of catechol-modified chitosan and Pluronic demonstrated rapid curing when heated to body temperature and showed strong adhesion (up to 18.5 kPa) to subcutaneous tissue.<sup>148</sup> Incorporation of thermo-responsive Pluronic copolymers into hydrogel systems can improve mechanical properties when the hydrogel is heated above its transition temperature.<sup>149</sup> Catechol-modified chitosan-Pluronic hydrogel exhibited excellent anti-bleeding properties in a hemorrhaging liver model in rat, reducing blood loss from 1000 mg to 250 mg after administration.<sup>148</sup> This hydrogel rapidly solidified, attached strongly to the tissue at the hemorrhage site, and acted as a physical barrier to stop the blood loss. In another study, chitosan modified with both catechol and ethylene glycol demonstrated hemostatic properties with a reduced immune response associated with catechol-modified chitosan.<sup>165</sup> However, glycol modification did not significantly improve the adhesive and hemostatic properties of the hydrogels when compared with the unmodified catechol-chitosan hydrogels.<sup>148,165</sup>

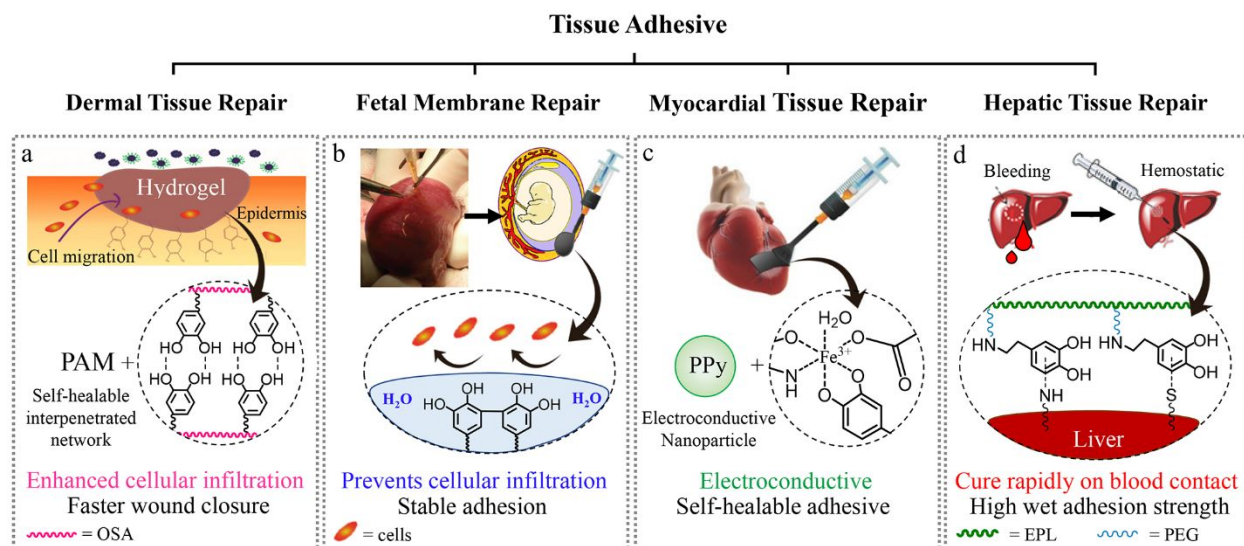


**Figure 17.** Schematic representation of catechol-functionalized hydrogels for tissue adhesives. (a) Adhesive designed for dermal adhesive repair consisted of interpenetrated network with self-healing property and the ability to enhance cellular infiltration. Reproduced with permission from ref. 164. Copyright 2018 American Chemical Society. (b) For fetal membrane repair, catechol cross-linking was used to design a hydrophilic hydrogel that prevented cellular infiltration. Reproduced with permission from ref. 168. Copyright 2013 Elsevier. (c) For myocardial tissue adhesive, catechol-metal ion complexation and electroconductive PPy nanoparticles were used to develop a nanocomposite self-healable electroconductive hydrogel. Reproduced with permission from ref. 169. Copyright 2018 Wiley-VCH. (d) For hepatic tissue repair, catechol-PEG-EPL was used to design an adhesive that rapidly cured on blood contact. Reproduced with permission from ref. 170. Copyright 2017 Wiley-VCH.

In one interesting design, the surface of a needle was coated with a thin homogenous film of the partially oxidized catechol-functionalized chitosan.<sup>166</sup> The film thickness was around 20–26  $\mu\text{m}$  depending on the needle gauge. The solid film converted to a soft gel-like material after incubation in phosphate buffered saline and further converted to a mechanically robust gel when exposed to blood plasma. The elastic modulus of the gel increased from 5 kPa to 93 kPa during this transition then slid off the needle and effectively sealed the puncture hole created by the needle. This self-sealing needle exhibited excellent hemostatic activity after intravenous and intramuscular punctures in animal models, as well as jugular vein puncture in hemophilic mice.

### 6.1.2 Dermal tissue repair

Dermal wounds are one of the most common injuries with varying degrees of severity, ranging from an insignificant small scratch to life-threatening large skin wounds with multiple complications.<sup>192</sup> The main requirements in the design of dermal adhesives include strong adhesive properties, mechanical strength, and biocompatibility. For major wounds, the adhesive must retain moisture at the wound site while allowing the wound to irrigate and drain sufficiently to prevent complications such as sepsis and tissue death.<sup>192,193</sup> Clinically, hydrogels and hydrogel adhesives are extensively used as wound debriding agents, moist dressings, and components of pastes for wound care.<sup>203</sup> They generally do not absorb moisture from wounds and are suitable for use in dry



wound and burn wound treatment as a moisture donor, which can help accelerate wound healing through wound autolytic debridement and moisture regulation.

Polydopamine was combined with polyacrylamide (PDA-PAM) to form a tough, self-healing adhesive hydrogel.<sup>142</sup> PDA-PAM demonstrated the ability to repeatedly adhere to skin, and to resist cyclic loading, which is ideal for an adhesive that is exposed to a dynamic environment during tissue repair. PDA-PAM also accelerated wound closure to 15 days in a full-thickness dermal wound model in rat. The hydrogel treatment reduced inflammatory cell recruitment and promoted the formation of aligned collagen matrix and hair follicles. These observations demonstrated that PDA-PAM could potentially minimize scar tissue formation. A similar skin adhesive was prepared using dopamine-grafted oxidized sodium alginate and polyacrylamide (OSA-DA-PAM) to create a tough interpenetrated hydrogel network.<sup>164</sup> This adhesive demonstrated a tensile strength of 100 kPa and the ability to stretch to 2550% strain before failure. In addition, the presence of alginate supported fibroblast adhesion. The hydrogel also demonstrated the ability to encapsulate and release epithelial growth factor (EGF), which could potentially increase the rate of skin wound closure. In a rat dermal wound model, OSA-DA-PAM-treated wounds demonstrated accelerated wound closure and the presence of more mature fibroblasts and compact collagen fibers compared with untreated wounds.

### 6.1.3 Fetal membrane repair

Fetal membrane rupture is associated with 30–40% of preterm births and can, in some cases, lead to fetal death.<sup>204</sup> The ruptured fetal membrane can naturally heal if the rupture size is small. However, only 40% of large ruptures heal naturally due to slow healing of the membrane. For an adhesive to seal fetal membrane defects, it must form an immediate durable barrier to amniotic fluid and be non-toxic.<sup>167,205</sup> A series of polyethylene glycol-modified catechol (PEG-catechol) hydrogels was investigated as adhesives for the repair of fetal membrane defects.<sup>167,206,207</sup> These PEG-catechol adhesives were non-degradable, which is preferable for long term sealing without relying on the fetal membrane to regenerate.<sup>206</sup> PEG-catechol demonstrated sufficient burst strength (45 mbar) and stretchability (94% strain before failure) needed to close the fetal membrane.<sup>167</sup> In addition, PEG-catechol did not exhibit cytotoxicity in culture. In an *in vivo* investigation, a PEG-catechol adhesive demonstrated a comparable performance to commercially available fibrin sealant, while preventing cellular infiltration into the adhesive network.<sup>205</sup> The reported lack of cellular infiltration is beneficial as it allows the non-degradable matrix to act as a plug for a prolonged period of time.

### 6.1.4 Myocardial tissue repair

Myocardial infarction (MI) is the leading cause of death worldwide, with more than 3 million cases in the United States alone.<sup>208</sup> Without proper intervention, remodeling of heart tissue can result in the loss of function, which leads to heart deformity, subsequent infarction incidences, and diminished quality of life.<sup>208,209</sup> One approach aimed at reducing subsequent incidences of MI involves cardiac rehabilitation therapy using an electroconductive patch to train and regain heart

tissue function.<sup>209</sup> However, fixing conductive patches to the myocardium through conventional surgical suture can induce additional trauma and inflammatory response, which negatively affects the healing process.<sup>190</sup> Hyperbranched polyaminoester modified with catechol has been loaded with polypyrrole nanoparticles to create an electroconductive adhesive.<sup>169</sup> This hydrogel solidified through oxidative cross-linking of catechol moieties and cured rapidly in a moist environment and demonstrated strong adhesion to porcine myocardium tissue (90.8 kPa). The electrical conductivity of the hydrogel was found to be  $6.5 \times 10^{-4} \text{ S cm}^{-1}$ , which is comparable to that of native myocardial tissue ( $1 \times 10^{-4} \text{ S cm}^{-1}$ ). When the adhesive was painted on an induced MI in rat, the adhesive fully integrated with the heart tissue. Moreover, the electrical conductivity of the adhesive allowed the myocardial tissue to beat in synchronicity with the surrounding healthy heart tissue. After four weeks of treatment, the infarction area was significantly reduced, with minimal fibrosis and heart deformation.<sup>169</sup>

### 6.1.5 Hepatic tissue repair

Hepatic tissue is blood-rich and highly prone to hemorrhage with minimal trauma. Conventionally, when liver trauma occurred, drainage, suturing, and cauterization were employed to stop the hemorrhage.<sup>210</sup> Although hepatic tissue is a unique tissue that can undergo full regeneration over time, hepatocyte transplantation can be required in the event of excessive loss of function.<sup>211</sup>  $\epsilon$ -poly-L-lysine (EPL) modified with catechol has demonstrated the ability to stop liver hemorrhaging in mouse.<sup>170</sup> EPL-modified catechol was found to reduce bleeding from 320 mg to 50 mg within 120 seconds of application. EPL-catechol hydrogel demonstrated a two order of magnitude stronger adhesion (150 kPa) when compared with commercial fibrin glue (5 kPa), which is commonly used to stop liver hemorrhage.<sup>212</sup> However, the mechanism of the hemostatic effect of EPL-modified hydrogel is not yet known.

## 6.2 Antifouling and antimicrobial applications

Cellular adhesion, protein deposition, and platelet activation are the main causes of implantable device failure.<sup>213,214</sup> In addition, microbes can colonize rapidly on device surfaces, leading to device failure as well as life-threatening sepsis.<sup>214</sup> One strategy for minimizing surface fouling is to functionalize surfaces with antifouling polymers such as PEG and other hydrophilic polymers, which can reduce the adsorption of proteins,<sup>215</sup> cells,<sup>216</sup> and microbes.<sup>217,218</sup> These hydrophilic polymers strongly couple water molecules, thus limiting the access of approaching cells and macromolecules to the surface adsorption sites.<sup>219,220</sup> Other strategies for creating antimicrobial biomaterials have involved the use of cationic polymers or metal ions that disrupt the cell membrane, as well as materials that release an antibiotic agent. Here, we describe and discuss catechol-modified antifouling and antimicrobial coatings, metal ion and nanoparticle containing hydrogels, and hydrogels that utilized the biocidal properties of catechol for antimicrobial applications.

### 6.2.1 Antifouling and ionic antimicrobial hydrogel coatings

Poly[(N-isopropylacrylamide)-co-(N-3,4-dihydroxyphenethyl acrylamide)]-b-poly(ethylene oxide)-b-poly[(N-isopropylacrylamide)-co-(N-3,4-dihydroxyphenethyl acrylamide)] (DNODN) is a tri-block copolymer that contains a hydrophilic PEG mid-block flanked by terminal blocks that contain catechol side chains and thermally-responsive poly(N-isopropylacrylamide) (poly(NIPAM)).<sup>171</sup> The polymer forms an injectable, shear-thinning hydrogel, which solidifies through non-covalent interactions (e.g., hydrogen bonding or  $\pi$ - $\pi$  interaction) between catechol moieties. The reversibility of the hydrogel during cyclic tests suggested that NIPAM also contributes to curing through hydrophobic interaction at an elevated temperature. A DNODN hydrogel-coated glass surface effectively prevented the adhesion of human colorectal cancer (Caco-2) cells. Similarly, an ABA triblock copolymer comprising a catechol-functionalized PEG-based A block and quaternized B block (poly([2-(methacryloyloxy)-ethyl] trimethylammonium iodide)) also demonstrated the ability to function as an injectable adhesive hydrogel with both antifouling and antibacterial properties.<sup>172</sup> The PEG-PMETA coating prevented the adhesion of Caco-2 cells. In addition, the hydrogel contained cationic trimethylammonium side chains that killed bacteria through the disruption of the bacterial cell membrane, with a 99.8% killing rate on *Escherichia coli*.<sup>172</sup> Similarly, EPL-catechol effectively killed 95% and 100% of *E. coli* and *Staphylococcus aureus*, respectively, potentially as a result of the cationic side chain of lysine in EPL.<sup>170</sup>

A similar antimicrobial effect can be achieved by the incorporation of weak organic acids with high carboxyl moiety content, such as citric acid. Undecylenate citric acid-containing catechol-citrate-PEG hydrogel suppressed the growth of both *S. aureus* and *E. coli*.<sup>173</sup> Citric acid contains high amounts of free carboxyl groups that disrupt cell walls and metabolic cycles by lowering the local pH, suppressing nicotinamide adenine dinucleotide (NADH) oxidation, and chelating metal ions in the cell wall. While metabolically toxic to bacteria, citric acid is noncytotoxic and considered biocompatible.<sup>173</sup> Catechol-citrate-PEG hydrogel can also be used to incorporate 10-undecenoyl, an antifungal drug, which demonstrated antifungal activity against *Candida albicans*.

### 6.2.2 Metal ion and nanoparticle-containing hydrogels

Metal ions such as silver, zinc, and copper have innate antibacterial properties, as they interfere with cell function through a competitive protein complexation mechanism.<sup>177,221</sup> Catechol chelates metal ions and sequesters these ions into the adhesive hydrogel.<sup>92</sup> During the oxidation of catechol, silver nitrate can be reduced to form silver nanoparticles, which are subsequently deposited into catechol-containing adhesives or coatings.<sup>174,222</sup> Silver nanoparticle-incorporated hydrogel was shown to be biostatic when tested against *E. coli*, *S. aureus*, and *Pseudomonas aeruginosa*.<sup>174</sup> The incorporation of the nanoparticles also increased the storage modulus of the hydrogel by one order of magnitude,<sup>174</sup> possibly as a result of interfacial binding between network-bound catechol and the incorporated nanoparticles.<sup>223,224</sup>

### 6.2.3 Biocidal properties of catechol

Reactive oxygen species (ROS) (e.g., superoxide, hydrogen peroxide ( $\text{H}_2\text{O}_2$ )) have numerous biological functions and are widely used as disinfectants.<sup>225</sup> During catechol oxidation, ROS such as superoxide and  $\text{H}_2\text{O}_2$  are generated as byproducts (Figure 18).<sup>226,227</sup> Catechol-modified microgel can be activated to generate  $\text{H}_2\text{O}_2$  of up to 4 mM under physiological conditions through simple hydration.<sup>175</sup> These microgels demonstrated the ability to completely prevent colony formation of both *E. coli* and *Staphylococcus epidermidis* within 24 hours and effectively inactivated the infectivity of both enveloped bovine viral diarrhea virus and non-enveloped porcine parvovirus. By tuning the oxidation state of the catechol using the solution pH, these microgels can be repeatedly activated (pH 7.4) and deactivated (pH 3.5) for on-demand generation of  $\text{H}_2\text{O}_2$ .<sup>175</sup>

PEG-catechol forms an adhesive hydrogel through oxidative cross-linking of the terminal catechol moieties.<sup>228,229</sup> PEG end-modified with 2-chloro-4,5-dihydroxyphenylalanine (Cl-DOPA) also demonstrated similar oxidant-induced curing behavior.<sup>176</sup> In addition, hydrogel coatings containing Cl-DOPA also prevented the adhesion of *E. coli* by up to 90%,<sup>176</sup> possibly as a result of the antibacterial properties of Cl-DOPA.<sup>230</sup>

Tannin is a polyphenol that also demonstrates antimicrobial properties.<sup>231</sup> Tannin comprises three aromatic rings with triol end groups, which can participate in redox chemistry and oxidation-induced polymerization similarly to catechol. These characteristics enable tannin to function as an effective adhesive moiety with added mild antimicrobial properties.<sup>177</sup> The antimicrobial mechanism of tannin is potentially associated with the cell wall complexation of oxidized tannins. Additionally, tannin-containing adhesive can reduce silver nanoparticles to further improve their antimicrobial properties.<sup>177</sup> This composite adhesive inhibited nearly 100% of both *S. aureus* and *E. coli* and effectively killed *C. Albicans*.

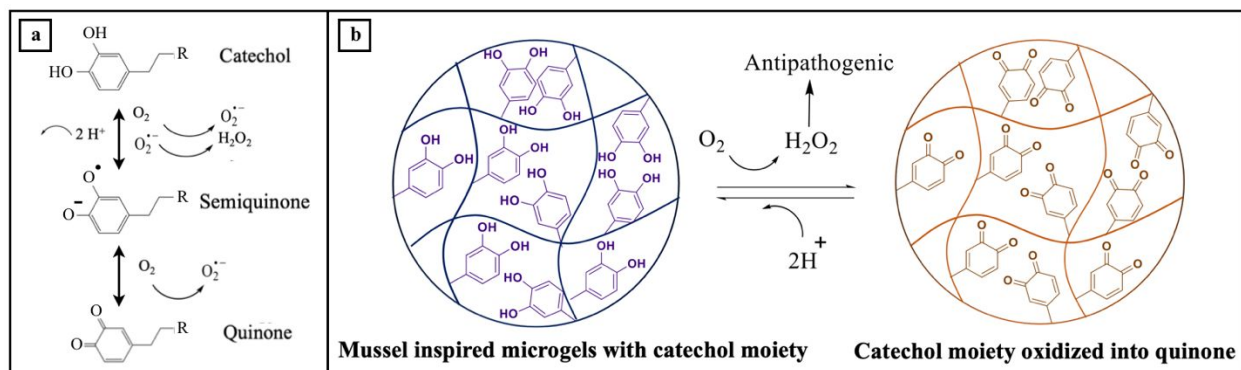


**Figure 18.** (a) Proposed mechanism of catechol oxidation and  $\text{H}_2\text{O}_2$  generation. (b) Schematic illustration of recyclable catechol-containing microgels. The dried microgels were hydrated in neutral to alkaline solution to generate  $\text{H}_2\text{O}_2$ . Reproduced with permission from ref. 175. Copyright 2019 Elsevier.

### 6.3 Drug Delivery

Oral and intravenous drug delivery are the most common methods for drug administration.<sup>178</sup> Drug delivery through mucosal membranes is also effective when the drug is unsuited for other administration routes, for example if they are susceptible to erosion or

degradation in the digestive system.<sup>231,232</sup> A successful drug delivery system must satisfy several design criteria including; ability to deliver a drug to a specific tissue to minimize side reactions associated with the drug,<sup>187,233</sup> tunable drug release, prolonged drug retention to deliver the drug at the optimal concentration,<sup>178</sup> and the drug carrier must be biocompatible and biodegradable. Here, we describe catechol-functionalized hydrogels designed for drug delivery applications, including mucoadhesive drug delivery systems, drug release through reversible boronic-catechol complexation, and catechol-containing capsules (Figure 19).

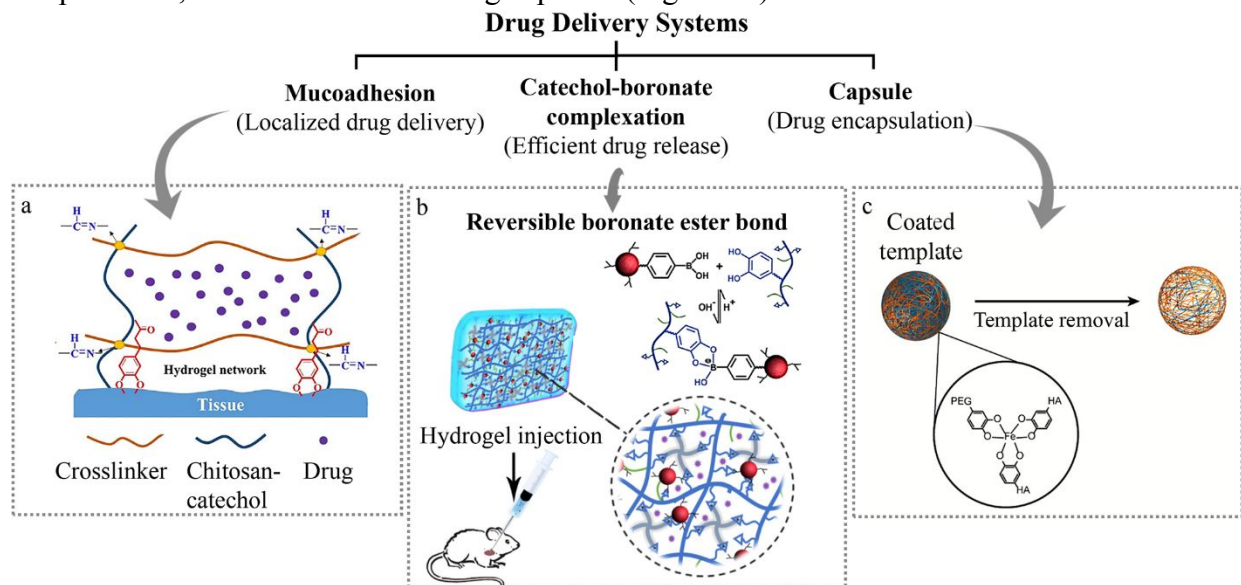


**Figure 19.** Schematic representation of catechol-functionalized hydrogels for drug delivery applications: (a) A catechol-containing drug carrier demonstrated increased mucoadhesive properties. Reproduced with permission from ref. 179. Copyright 2019 Elsevier. (b) Reversible catechol boronate complexation was used to design a hydrogel with pH-responsive drug release behavior. Reproduced with permission from ref. 183. Copyright 2018 American Chemical Society. (c) Catechol-metal ion complexation was used to develop a metal-phenolic network (MPN) capsule. Reproduced with permission from ref. 187. Copyright 2016 American Chemical Society.

### 6.3.1 Mucoadhesive drug carriers

Drug delivery through mucosal membranes such as buccal, gastrointestinal, and ocular mucosa requires the drug carriers to adhere to the local mucosal membrane or mucosal fluid through covalent (e.g., disulfide bridging) or non-covalent (e.g., electrostatic interactions, hydrophobic interactions, or hydrogen bonding) interactions.<sup>234</sup> Several mucoadhesive biopolymers such as chitosan, alginate, and hyaluronic acid (HA) have been extensively studied for the design of mucoadhesive drug delivery systems owing to their mucoadhesive properties and known biocompatibility.<sup>234</sup> However, these polymers are still limited by relatively low mucoadhesion, weak mechanical properties, and fast degradation rates, which result in limited drug retention time. Catechol conjugation is a simple and promising approach for increasing the mucoadhesive properties of a material.<sup>235</sup>

Catechol-functionalized chitosan hydrogels were developed for buccal<sup>180</sup> and colonic<sup>178,179</sup> drug delivery applications (Figure 19A). Catechol-chitosan hydrogels were further cross-linked with genipin (GP)<sup>180</sup> or oxidized pullulan (OP),<sup>179</sup> which exhibited enhanced mucoadhesive and

mechanical properties. A GP-cross-linked hydrogel loaded with lidocaine hydrochloride monohydrate, a local anesthesia drug, successfully delivered the loaded drug when attached to rabbit buccal mucosal membrane with no evidence of inflammation or foreign body reaction.<sup>180</sup> A similar GP-cross-linked catechol-chitosan hydrogel was used for rectal delivery of sulfasalazine for the treatment of ulcerative colitis, an inflammatory condition of the bowel.<sup>178</sup> The sulfasalazine-loaded hydrogel was demonstrated to be more effective and safer for the treatment of ulcerative colitis when compared with oral administration of the drug. The drug-free catechol-chitosan hydrogel was shown to contribute to the healing process of the colitis, possibly as a result of the anti-inflammatory and scavenging activity of the catechol.<sup>225,236</sup> The swelling behavior of chitosan is pH-dependent, which can be used to control the drug release profile. Catechol-chitosan hydrogel-loaded with doxorubicin (DOX), an anticancer drug, demonstrated faster drug release in mildly acidic conditions (pH 5.5) than at pH 7.4.<sup>180</sup> This pH-responsive behavior could potentially be triggered by the more acidic environment that surrounds cancer cells. DOX-loaded hydrogel inhibited the proliferation of human colon cancer cells (HCT116) compared with that of the drug-free hydrogel.

Catechol-HA conjugate was coupled with thiol-end capped Pluronic copolymers to produce an injectable mucoadhesive hydrogel for drug delivery applications.<sup>147</sup> The incorporation of Pluronic copolymer promoted rapid sol-gel transition behavior in response to temperature. The addition of catechol moieties increased the adhesion strength of the hydrogel to more than 7 kPa when tested *in vitro*, which is significantly higher than that of the catechol-free hydrogels.<sup>147</sup> Hydrogels composed of catechol-HA and Pluronic exhibited excellent stability and mucoadhesive properties when injected subcutaneously in mice, and 78 wt% of the originally injected hydrogel was retrieved after 21 days of implantation. These excellent mucoadhesive properties and rapid curing properties are attractive for prolonged drug delivery applications.

Catechol-modified alginate was developed as an injectable mucoadhesive hydrogel to serve as an alternative to drug eluting stents for the treatment of vulnerable atherosclerotic plaques.<sup>181</sup> Corticosteroid was encapsulated within catechol-alginate hydrogel, which was painted inside the blood vessel walls of an atherosclerosis model in mouse. The adhesive hydrogel exhibited strong, long-term adhesion to the vessel wall and did not illicit a chronic inflammatory response. In addition, the hydrogel demonstrated reduced inflammation-related biomarkers, including macrophage and plasma cytokines. Therefore, this mucoadhesive hydrogel can potentially be used to deliver drugs for the treatment of diseased vasculatures.

### 6.3.2 Catechol-boronate complexation-based drug release

Catechol forms pH-dependent, reversible complexes with boronic acid.<sup>162</sup> Bortezomib (BTZ) is a dipeptidyl anticancer drug that contains a terminal boronic acid compound,<sup>237</sup> which can bind reversibly to catechol. Catechol-boronate complex is stable at physiological pH (7.4), which allowed BTZ to bind to the catechol-containing drug carrier (Figure 20B).<sup>238</sup> Dissociation of catechol-boronate complexation can be triggered in the acidic environment associated with cancer cells, which leads to the controlled and targeted release of BTZ. BTZ-loaded PDA

nanoparticles have been encapsulated in a 3D hydrogel network.<sup>182</sup> This composite hydrogel exhibited excellent pH-responsive drug release behavior. In mildly acidic conditions (pH 5), 68% of the initial BTZ loaded was released from the hydrogel after 72 hours, which was significantly higher than the amount of drug released at pH 7.4 (less than 20%). This controlled drug release effectively reduced the viability of CT26 colon cancer cells.<sup>182</sup>

DOX was encapsulated in a phenylboronic acid-containing nanogel consisting of poly(acrylic acid-co-4-vinylphenylboronic acid), which was further incorporated into an injectable catechol-containing hydrogel consisting of poly(N-(3,4-dihydroxyphenethyl)methacrylamide-co-poly(ethylene glycol)methyl ether methacrylate) (Poly(DMA-co-PEGMA)).<sup>183</sup> The nanogel contained a large number of carboxyl groups, which were used to load a considerable amount of drug containing amino groups, such as DOX, through electrostatic interactions.<sup>239,240</sup> In mildly acidic conditions, dissociation of the catechol-boronate linkage between the hydrogel and nanogel and the ionization between the carboxylic and amino groups between the nanogel and DOX, resulted in the sustained release of the loaded drug from the composite hydrogel.<sup>183</sup> At pH 6.5, 66.3% of the initially loaded drug was released within 14 days while the drug release significantly reduced to 15.8% at pH 7.4. This pH-responsive drug release behavior is potentially suitable for delivering therapeutic drugs for cancer treatment.

### 6.3.3 Capsules

Nano- and micron-scaled polymeric capsules have been used as drug delivery carriers.<sup>241</sup> Both the shell and core of a capsule can be independently loaded with drug or functionalized with stimuli-responsive functional groups for controlled and targeted drug delivery. The polymerization of dopamine on sacrificial templates based on micron-sized particles was used to create a PDA capsule with controllable size and wall thickness after removing the template.<sup>184,185</sup> The capsules were successfully loaded with a cargo and exhibited a release profile that was dependent on the biodegradation properties of the capsule. The incorporation of poly(L-glutamic acid) (PGA) into the PDA capsules promoted the degradation behavior and a faster drug release profile.<sup>185</sup> A pH-responsive capsule was developed by immobilizing DOX conjugated poly(methacrylic acid) onto the PDA capsule using an acid-labile hydrazone bond.<sup>186</sup> Degradation of the hydrazone bond in an acidic environment (pH 5) triggered the release of up to 85% of the initially loaded drug over 12 hours. At pH 7.4, the drug release rate was slow and reached less than 20%. This pH dependent drug release profile is potentially suitable for designing drug carriers for cancer therapy.

pH responsive catechol-metal ion complexation has been exploited to develop a series of structurally diverse capsules.<sup>242,243</sup> These so-called metal-phenolic network (MPN) capsules (Figure 20c) have been prepared using tannic acid and a wide range of metal ions including iron and aluminum.<sup>243,244</sup> These capsules are relatively stable at neutral pH owing to the formation of complexes with higher stoichiometry (e.g., 3:1 TA: Al<sup>3+</sup> ion).<sup>244</sup> At lower pH (5), the formation of a complex with a reduced stoichiometry (1:1 TA: Al<sup>3+</sup> ion) resulted in the rapid degradation (up to 80% of the capsule in 48 hours) and release of the encapsulated drugs. MPN capsules with high cancer cell targeting efficacy were created using a combination of catechol-modified HA and

PEG.<sup>187</sup> The incorporation of PEG minimized the nonspecific adsorption of proteins and cells, while HA enhanced the ability of the capsules to target and bind cancer cells that overexpressed the CD44 receptor. An optimized capsule was developed by balancing the HA to PEG content to achieve high specific targeting of CD44 positive cancer cells, while minimizing the non-specific binding of CD44 negative cells.

#### 6.4 Cell encapsulation and delivery

Cell encapsulation is an alternative and versatile approach for the sustained delivery of therapeutic biomolecules that are continuously released by the encapsulated cells in a controlled manner.<sup>245</sup> A successful cell encapsulation and delivery system requires a polymer network with high biocompatibility to achieve a favorable cell survival rate, tunable swelling behavior for efficient nutrient and waste transfer, appropriate mechanical properties, and the ability to bind to wet tissue surfaces.<sup>188,246,247</sup> Hydrogels are typically used for cell encapsulation and delivery owing to their high water content and porous 3D structure, which provides a physiologically favorable environment for cell survival and growth, while avoiding undesirable immune responses.<sup>245</sup> Biocompatible hydrogels including HA,<sup>248</sup> alginate,<sup>249</sup> and PEG<sup>250</sup> have been developed for drug and cell therapy. However, curing these hydrogels required either UV-initiated polymerization or the addition of a reagent (e.g., divalent cations), which often negatively affect cell viability and proliferation.<sup>188,190</sup> In addition, these hydrogels lacked the strong adhesion and mechanical properties necessary for cell immobilization and deposition.<sup>146,189</sup> Various catechol-modified hydrogels designed for cell encapsulation and delivery are described here.

Catechol-functionalized alginate can solidify quickly through catechol-catechol cross-linking, without the need for divalent cations.<sup>188</sup> Catechol-alginate hydrogel exhibited a significantly higher swelling rate (230%) compared with catechol-free hydrogel (60%), which led to more efficient mass exchange. This hydrogel exhibited a maximum storage modulus of 6 kPa, which is a favorable stiffness range for the proliferation and differentiation of neural or adipocyte cells.<sup>188,251</sup> The hydrogel was able to successfully encapsulate human neural stem cells (hNSCs) and human umbilical vein endothelial cells (HUVECs) while maintaining significantly higher cell viability (99–100%) compared with alginate hydrogel cured using divalent cations (80–86%).<sup>188</sup> The hydrogel demonstrated negligible cytotoxicity and inflammatory responses when evaluated using a subcutaneous implantation model in mouse.

A catechol-PEG hydrogel was developed to immobilize islet cells for the treatment of type I diabetes.<sup>146</sup> This hydrogel exhibited minimal acute and chronic inflammatory responses when implanted in a healthy mouse. Catechol-PEG cured rapidly and efficiently to immobilize islet cells on the surface of extrahepatic tissues in a Streptozotocin-induced diabetic mouse model. Mice that received the islet cell transplant demonstrated normoglycemic recovery for over 100 days, which makes this hydrogel a promising model for pancreatic islets.

Catechol-functionalized HA hydrogels have also been reported for cellular encapsulation. Catechol-HA hydrogels exhibited excellent biocompatibility toward different types of cells including hNSCs,<sup>189</sup> human primary hepatocytes (hHEPs),<sup>190</sup> and human adipose-derived stem



cells (hADSCs).<sup>190,191</sup> These primary cells and stem cells are particularly vulnerable to microenvironmental changes during the curing of the hydrogel, which can negatively affect cell viability and proliferation.<sup>252</sup> Cells encapsulated in catechol-HA hydrogel exhibited improved viability compared with those that were encapsulated in conventional HA hydrogels.<sup>190,191</sup> In an ischemic mouse model, the transplanted hADSCs migrated into the ischemic tissue, leading to angiogenesis, as the level of secreted vascular endothelial growth factor (VEGF) was significantly higher than those in catechol-free adhesive.<sup>190</sup> Similarly, for hepatocyte transplantation, the encapsulated hHEPs migrated into the hepatic tissue within 3 days of implantation, resulting in improved hepatic function based on the albumin level measurements.<sup>190</sup> Transplantation of hADSCs using HA-catechol hydrogel also improved osteogenesis in a critical-sized calvarial bone defect model in mice.<sup>191</sup> Catechol-modified HA provides a hydrogel platform that can be used to deliver therapeutic cells for various cell and tissue engineering applications.

## 7. Current challenges and future opportunities

Finally, we would like to make a few remarks on the current challenges and research opportunities. The research and development of catechol-containing hydrogels and adhesives have expanded rapidly in recent years, and our understanding of their interfacial chemistry, adhesive properties, and applications is also significantly improving. However, there are issues limiting the transfer of catechol-containing wet adhesives into real world applications. These limitations include slow curing kinetics, uncertain biocompatibility, bonding reliability on varied surface quality and environments, and the desired reversibility.

Hydrogels capable of rapid and robust wet adhesion are beneficial for many applications such as surgical hemostasis and underwater sealing. The relatively slow kinetics of catechol curing remains an unmet challenge. Additionally, and the catechol curing conditions (e.g. oxidant, elevated pH, etc.) are not always compatible with the targeted applications, such as biomedical applications. Given the versatile roles and reactivity of catechol in wet adhesion, opportunities may lie in the combination of catechol chemistry with other high efficacy polymer crosslinking chemistry, clickable coupling reactions and multiplex supramolecular interactions. Catechol-containing copolymers, blends, and composites are also needed to integrate different functionalities into one single hydrogel system. With recent progress in the synthesis and properties of sequence defined polymers,<sup>253,254</sup> there are emerging opportunities in controlling local sequences of catechol-containing copolymers for modulated chemical environment of catechol moieties, thus improving control over catechol curing kinetics. Moreover, topology and microstructure engineering of hydrogels should be considered to amplify or accelerate the catechol curing effect through, for example, the enlarged surface area or hybrid interfaces. New chemistry promoting catechol curing under mild conditions is also in demand.

In addition to curing kinetics, currently, the synthesis of catechol-containing polymer involves considerable synthetic complexity such as specialized chemical techniques, catechol protection, de-protection and grafting, all of which reduces the accessibility of these adhesive hydrogels.<sup>255</sup> Smart hydrogel adhesives that exhibit tunable functionalities—other than simple

mechanical properties—have not been widely investigated for task-specific uses. One of the remaining challenges is correlating the properties of catechol polymer chain with the optimized adhesive properties. This may require broadening our theoretical understanding of wet adhesion beyond modeling from an energetic perspective.

We have predominantly reviewed adhesive hydrogels designed for permanent adhesion. However, smart adhesives that provide temporary yet reversible adhesion in response to externally applied stimuli have potential applications across multiple disciplines. Smart adhesives that display tunable responsive and reversible adhesion in the presence of an external stimulus such as temperature, pH, or ionic strength are favored. Among these factors, light irradiation is most effective, and can be utilized a wet condition to induce strong and on-demand attachment or detachment on various substrates.<sup>256–258</sup> This type of non-invasive tuning of adhesive property is especially meaningful in a wide range of medical procedures. In addition to the light effect, various physiological parameters, such as glucose concentration, the presence of enzymes, and pH variations are potentially desired triggers for tuning the adhesion behaviors of smart hydrogels.

For biomedical applications, biocompatibility of the adhesive is one of the top priorities. As such, biopolymers such as proteins and polysaccharides appear to be suitable sources for fabricating biomedical adhesives. Compared with synthetic polymers that are bioinert, these biopolymers provide added benefits of enhanced bioactivity, ability to promote cell adhesion, and biodegradability.<sup>196</sup> However, just because an adhesive is derived from a natural source, it does not guarantee that the adhesive is safe. The biological-based tissue adhesives are exemplified by fibrin glues, which utilize the final stages of the blood coagulation cascade to form a fibrin network adhesive and is widely used as a tissue sealant.<sup>259</sup> However, fibrin glue that consists of human-derived components are a potential source of viral transmission (i.e., HIV, hepatitis).<sup>260</sup> Additionally, it is necessary to have a complete understanding on the effects of the curing chemistry, byproduct generation, and degradation products on the biological system of the targeted application. Different biological systems may also respond differently to these reaction products. For example, catechol generates  $\text{H}_2\text{O}_2$  as a by-product during the process of curing.<sup>228</sup> Given that different cell types respond differently to oxidative stress,<sup>261</sup> it is necessary to tune the release of  $\text{H}_2\text{O}_2$  from catechol-containing hydrogels for different applications. The biocompatibility of the adhesive hydrogels should be evaluated following standardized guidelines (i.e., ISO-10933: Biological evaluation of medical devices)<sup>262</sup> to facilitate regulatory approval.

During the past decade, scientists in both academia and industry have recognized the need to push for advances in adhesive hydrogels; the field has witnessed a dramatic expansion of publications and patent applications, demonstrating the tremendous efforts of researchers worldwide in bringing adhesive hydrogels towards usage in daily life. To date, a variety of hydrogel-based bioadhesives are commercially available (e.g., Coseal, Baxter Healthcare Corporation and DuraSeal, Integra LifeSciences). The continuous development of hydrogel products sets new standards for their properties; many of today's challenges lie in the development of adhesive hydrogel materials with controllable adhesion, structures, and interfaces. New classes of

biomimetic hydrogels are poised to provide seamless integration between desired functionalities and advanced properties.

## 8 Summary

This review compiles state-of-the-art examples and details progress in the design and development of adhesive hydrogel materials based on mussel-inspired catechol chemistry. From a fundamental perspective, two main aspects have been examined: the role of water in undermining adhesion in hydrogels and the adhesive mechanism involving catechol-containing adhesives and coatings. By employing catechol moieties to engineer hydrogels, strong and robust underwater bonding between hydrogels and a diverse range of surfaces has been developed. We provide an overview of the synthetic approaches, fabrication techniques, and characterization methods for catechol-functionalized adhesive hydrogels, as well as the effects of interfaces and nanostructures on their adhesive properties. The intrinsic properties of adhesive hydrogels have expanded their potential in a variety of biomedical applications including tissue repair and regeneration, antifouling and antimicrobial applications, drug delivery, and cell encapsulation and delivery. The insights presented on these topics will provide rational guidelines for the design of future functional hydrogels.

## Conflicts of interest

There are no conflicts to declare.

## Acknowledgements

This work is supported by the Natural Science Foundation of Jiangsu Province (grant BK20180407), the National Natural Science Foundation of China (grants 51903047 and 51731004) and the Fundamental Research Funds for the Central Universities. Q. Z. acknowledges the financial support from the 1000 Young Talent program and the Huazhong University of Science and Technology (grant 3004013118). B. Z. acknowledges the financial support from the Natural Sciences and Engineering Research Council of Canada (grants RGPIN-2019-04650 and RGPAS-2019-00115). B. P. L. acknowledges the financial support from the National Institutes of Health (grant R15GM104846), the Office of Naval Research (grant N00014-16-1-2463), and the Office of the Assistant Secretary of Defense for Health Affairs through the Defense Medical Research and Development Program (grant W81XWH1810610).

## References

- 1 H. Yuk, B. Lu and X. Zhao, *Chem. Soc. Rev.*, 2019, **48**, 1642–1667.
- 2 Y. S. Zhang and A. Khademhosseini, *Science*, 2017, **356**, 3627.
- 3 D. Caccavo, S. Cascone, G. Lamberti and A. A. Barba, *Chem. Soc. Rev.*, 2018, **47**, 2357–2373.
- 4 P. Thoniyot, M. J. Tan, A. A. Karim, D. J. Young and X. J. Loh, *Adv. Sci.*, 2015, **2**, 1400010.
- 5 J. A. Yang, J. Yeom, B. W. Hwang, A. S. Hoffman and S. K. Hahn, *Prog. Polym. Sci.*, 2014, **39**, 1973–1986.
- 6 N. Sahiner, *Prog. Polym. Sci.*, 2013, **38**, 1329–1356.
- 7 J. A. Johnson, N. J. Turro, J. T. Koberstein and J. E. Mark, *Prog. Polym. Sci.*, 2010, **35**, 332–337.
- 8 C. R. Nuttelman, M. A. Rice, A. E. Rydholm, C. N. Salinas, D. N. Shah and K. S. Anseth, *Prog. Polym. Sci.*, 2008, **33**, 167–179.
- 9 D. J. Beebe, J. Moore, J. M. Bauer, Q. Yu, R. H. Liu, C. Devadoss and B. H. Jo, *Nature*, 2000, **404**, 588.
- 10 N. M. Sangeetha and U. Maitra, *Chem. Soc. Rev.*, 2005, **34**, 821.
- 11 L. A. Estroff and A. D. Hamilton, *Chem. Rev.*, 2004, **104**, 1201–1217.
- 12 W. Zhang, P. Feng, J. Chen, Z. Sun and B. Zhao, *Prog. Polym. Sci.*, 2019, **88**, 220–240.
- 13 A. Alam, Y. Zhang, H.-C. Kuan, S.-H. Lee and J. Ma, *Prog. Polym. Sci.*, 2018, **77**, 1–18.
- 14 F. Zhao, Y. Shi, L. Pan and G. Yu, *Acc. Chem. Res.*, 2017, **50**, 1734–1743.
- 15 A. Guiseppi-Elie, *Biomaterials*, 2010, **31**, 2701–2716.
- 16 W. E. Hennink and C. F. van Nostrum, *Adv. Drug Deliv. Rev.*, 2012, **64**, 223–236.
- 17 D. Buenger, F. Topuz and J. Groll, *Prog. Polym. Sci.*, 2012, **37**, 1678–1719.
- 18 T. R. Hoare and D. S. Kohane, *Polymer (Guildf.)*, 2008, **49**, 1993–2007.
- 19 B. Jeong, S. Wan and Y. Han, *Adv. Drug Deliv. Rev.*, 2002, **54**, 37–51.
- 20 G. Sun, Z. Li, R. Liang, L.-T. Weng and L. Zhang, *Nat. Commun.*, 2016, **7**, 12095.
- 21 T. Huang, H. Xu, K. Jiao, L. Zhu, H. R. Brown and H. Wang, *Adv. Mater.*, 2007, **19**, 1622–1626.
- 22 J. F. Feng, J. L. Chen, K. Guo, J. B. Hou, X. L. Zhou, S. Huang, B. J. Li and S. Zhang, *ACS Appl. Mater. Interfaces*, 2018, **10**, 40238–40245.
- 23 L. Han, X. Lu, K. Liu, K. Wang, L. Fang, L. T. Weng, H. Zhang, Y. Tang, F. Ren, C. Zhao, G. Sun, R. Liang and Z. Li, *ACS Nano*, 2017, **11**, 2561–2574.
- 24 Y. Zhou, W. Nie, J. Zhao and X. Yuan, *J. Mater. Sci. Mater. Med.*, 2013, **24**, 2277–2286.
- 25 F. Sun, C. Yang, W. Xu, Y. Liang, X. Chen, E. Liang, G. Wang, N. Zhou and J. Yi, *J. Mater. Chem. B*, 2019, **7**, 1996–2000.
- 26 C. Cui, T. Wu, F. Gao, C. Fan, Z. Xu, H. Wang, B. Liu and W. Liu, *Adv. Funct. Mater.*, 2018, **28**, 1–12.
- 27 Y. Wang, F. Huang, X. Chen, X. W. Wang, W. Bin Zhang, J. Peng, J. Li and M. Zhai, *Chem. Mater.*, 2018, **30**, 4289–4297.

- 28 C. Heinzmann, C. Weder and L. M. De Espinosa, *Chem. Soc. Rev.*, 2016, **45**, 342–358.
- 29 Y. Hong, F. Zhou, Y. Hua, X. Zhang, C. Ni, D. Pan, Y. Zhang, D. Jiang, L. Yang, Q. Lin, Y. Zou, D. Yu, D. E. Arnot, X. Zou, L. Zhu, S. Zhang and H. Ouyang, *Nat. Commun.*, 2019, **10**, 2060.
- 30 M. Rahimnejad and W. Zhong, *RSC Adv.*, 2017, **7**, 47380–47396.
- 31 J. H. Ryu, S. Hong and H. Lee, *Acta Biomater.*, 2015, **27**, 101–115.
- 32 T. Thiruselvi, S. Thirupathi Kumara Raja, R. Aravindhana, S. K. Shanuja and A. Gnanamani, *RSC Adv.*, 2016, **6**, 19973–19981.
- 33 M. Krosggaard, V. Nue and H. Birkedal, *Chem. - A Eur. J.*, 2016, **22**, 844–857.
- 34 J. Sedö, J. Saiz-Poseu, F. Busqué and D. Ruiz-Molina, *Adv. Mater.*, 2013, **25**, 653–701.
- 35 E. Faure, C. Falentin-Daudré, C. Jérôme, J. Lyskawa, D. Fournier, P. Woisel and C. Detrembleur, *Prog. Polym. Sci.*, 2013, **38**, 236–270.
- 36 B. P. Lee, P. B. Messersmith, J. N. Israelachvili and J. H. Waite, *Annu. Rev. Mater. Res.*, 2011, **41**, 99–132.
- 37 J. J. Wilker, *Nat. Chem. Biol.*, 2011, **7**, 579–580.
- 38 H. Yuk, T. Zhang, S. Lin, G. A. Parada and X. Zhao, *Nat. Mater.*, 2016, **15**, 190–196.
- 39 Q. Zhao, D. W. Lee, B. K. Ahn, S. Seo, Y. Kaufman, J. N. Israelachvili and J. H. Waite, *Nat. Mater.*, 2016, **15**, 407–412.
- 40 J. Li, A. D. Celiz, J. Yang, Q. Yang, I. Wamala, W. Whyte, B. R. Seo, N. V. Vasilyev, J. J. Vlassak, Z. Suo and D. J. Mooney, *Science*, 2017, **357**, 378–381.
- 41 H. Zeng, D. S. Hwang, J. N. Israelachvili and J. H. Waite, *Proc. Natl. Acad. Sci.*, 2010, **107**, 12850–12853.
- 42 H. Lee, S. M. Dellatore, W. M. Miller and P. B. Messersmith, *Science*, 2007, **318**, 426–430.
- 43 H. Lee, B. P. Lee and P. B. Messersmith, *Nature*, 2007, **448**, 338–341.
- 44 J. H. Waite, *Nat. Mater.*, 2008, **7**, 8–9.
- 45 A. Napolitano, V. Ball, C. Chen and M. J. Buehler, *Acc. Chem. Res.*, 2014, **47**, 3541–3550.
- 46 T. Nakamura, M. Hattori, H. Kawasaki, K. Miyamoto, M. Tokita and T. Komai, *Phys. Rev. E*, 1996, **54**, 1663–1668.
- 47 J. D. Andrade, S. M. Ma, R. N. King and D. E. Gregonis, *J. Colloid Interface Sci.*, 1979, **72**, 488–494.
- 48 K. Autumn, M. Sitti, Y. A. Liang, A. M. Peattie, W. R. Hansen, S. Sponberg, T. W. Kenny, R. Fearing, J. N. Israelachvili and R. J. Full, *Proc. Natl. Acad. Sci.*, 2002, **99**, 12252–12256.
- 49 M. Zhou, N. Pesika, H. Zeng, Y. Tian and J. Israelachvili, *Friction*, 2013, **1**, 114–129.
- 50 K. Y. Lee and D. J. Mooney, *Prog. Polym. Sci.*, 2012, **37**, 106–126.
- 51 A. Cholewinski, F. K. Yang and B. Zhao, *Langmuir*, 2017, **33**, 8353–8361.
- 52 F. J. Cedano-Serrano, U. Sidoli, A. Synytska, Y. Tran, D. Hourdet and C. Creton, *Macromolecules*, 2019, **52**, 3852–3862.
- 53 A. Xin, R. Zhang, K. Yu and Q. Wang, *J. Mech. Phys. Solids*, 2019, **125**, 1–21.

- 54 D. Gan, W. Xing, L. Jiang, J. Fang, C. Zhao, F. Ren, L. Fang, K. Wang and X. Lu, *Nat. Commun.*, 2019, **10**, 1487.
- 55 J. N. Israelachvili, *Intermolecular and Surface Forces*, Academic Press, 2011.
- 56 J. Yu, Y. Kan, M. Rapp, E. Danner, W. Wei, S. Das, D. R. Miller, Y. Chen, J. H. Waite and J. N. Israelachvili, *Proc. Natl. Acad. Sci.*, 2013, **110**, 15680–15685.
- 57 G. P. Maier, M. V. Rapp, J. H. Waite, J. N. Israelachvili and A. Butler, *Science*, 2015, **349**, 628–632.
- 58 J. N. Israelachvili, *Intermolecular and Surface Forces*. Elsevier, **2011**.
- 59 J. Saiz-Poseu, J. Mancebo-Aracil, F. Nador, F. Busqué, and D. Ruiz-Molina, *Angew. Chem. Int. Ed.*, 2019, **58**, 696-714.
- 60 H. J. Schneider and A. K. Yatsimirsky, *Chem. Soc. Rev.*, 2008, **37**, 263–277.
- 61 Y. Ahn, Y. Jang, N. Selvapalam, G. Yun and K. Kim, *Angew. Chemie Int. Ed.*, 2013, **52**, 3140-3144.
- 62 D. E. Packham, in *Handbook of Adhesion Technology*, eds. L. F. M. da Silva, A. Öchsner and R. D. Adams, Springer Berlin Heidelberg, Berlin, Heidelberg, **2011**, pp. 9–38.
- 63 A. N. Gent, *Langmuir*, 1996, **12**, 4492–4496.
- 64 D. E. Packham, in *Adhesion Science and Engineering*, Elsevier, **2002**, pp. 317–349.
- 65 P. Rao, T. L. Sun, L. Chen, R. Takahashi, G. Shinohara, H. Guo, D. R. King, T. Kurokawa and J. P. Gong, *Adv. Mater.*, 2018, **30**, 1801884.
- 66 P. Karami, C. S. Wyss, A. Khoushabi, A. Schmocker, M. Broome, C. Moser, P.-E. Bourban and D. P. Pioletti, *ACS Appl. Mater. Interfaces*, 2018, **10**, 38692–38699.
- 67 F. Yang, A. Cholewinski, L. Yu, G. Rivers and B. Zhao, *Nat. Mater.*, 2019, **18**, 874–882.
- 68 H. Yoshida, T. Hatakeyama and H. Hatakeyama, *J. Therm. Anal.*, 1993, **40**, 483–489.
- 69 J. H. Waite, *Integr. Comp. Biol.*, 2002, **42**, 1172–1180.
- 70 H. Schonhorn, *J. Plast. Film Sheeting*, 1985, **1**, 163–179.
- 71 L. C. Bradley, N. D. Bade, L. M. Mariani, K. T. Turner, D. Lee and K. J. Stebe, *ACS Appl. Mater. Interfaces*, 2017, **9**, 27409–27413.
- 72 R. Michel, L. Poirier, Q. van Poelvoorde, J. Legagneux, M. Manassero and L. Corté, *Proc. Natl. Acad. Sci.*, 2019, **116**, 738–743.
- 73 D. Jia, Y. Pang and X. Liang, *J. Polym. Sci. Part B Polym. Phys.*, 1994, **32**, 817–823.
- 74 T. Kurokawa, H. Furukawa, W. Wang, Y. Tanaka and J. P. Gong, *Acta Biomater.*, 2010, **6**, 1353–1359.
- 75 J. J. Sahlin and N. A. Peppas, *J. Biomater. Sci. Polym. Ed.*, 1997, **8**, 421–436.
- 76 S. Tamesue, T. Endo, Y. Ueno and F. Tsurumaki, *Macromolecules*, 2019, **52**, 5690-5697.
- 77 J. Yang, R. Bai and Z. Suo, *Adv. Mater.*, 2018, **30**, 1800671.
- 78 J. Yang, R. Bai, B. Chen and Z. Suo, *Adv. Funct. Mater.*, 2019, 1901693.
- 79 A. Cholewinski, F. K. Yang and B. Zhao, *Mater. Horizons*, 2019, **6**, 285–293.
- 80 S. O. Blacklow, J. Li, B. R. Freedman, M. Zeidi, C. Chen and D. J. Mooney, *Sci. Adv.*, 2019, **5**, eaaw3963.
- 81 R. Rahimi, S. Shams Es-haghi, S. Chittiboyina, Z. Mutlu, S. A. Lelièvre, M. Cakmak and

- B. Ziaie, *Adv. Healthc. Mater.*, 2018, **7**, 1800231.
- 82 Q. Zhang, X. Liu, L. Duan and G. Gao, *Chem. Eng. J.*, 2019, **365**, 10–19.
- 83 C. Loskofsky, F. Song and B. Z. Newby, *J. Adhes.*, 2006, **82**, 713–730.
- 84 D. Arunbabu, H. Shahsavan, W. Zhang and B. Zhao, *J. Phys. Chem. B*, 2013, **117**, 441–449.
- 85 K. J. Tong and D. M. Ebenstein, *JOM*, 2015, **67**, 713–719.
- 86 G. Sudre, L. Olanier, Y. Tran, D. Hourdet and C. Creton, *Soft Matter*, 2012, **8**, 8184.
- 87 K. R. Shull, *Mater. Sci. Eng. R Reports*, 2002, **36**, 1–45.
- 88 R. E. Webber and K. R. Shull, *Macromolecules*, 2004, **37**, 6153–6160.
- 89 H. Zhang, T. Zhao, B. Newland, W. Liu, W. Wang and W. Wang, *Prog. Polym. Sci.*, 2018, **78**, 47–55.
- 90 J. H. Waite and M. L. Tanzer, *Science*, 1981, **212**, 1038–1040.
- 91 J. H. Waite, *J. Exp. Biol.*, 2017, **220**, 517–530.
- 92 P. Kord Forooshani and B. P. Lee, *J. Polym. Sci. Polym. Chem.*, 2017, **55**, 9–33.
- 93 W. Wei, J. Yu, C. Broomell, J. N. Israelachvili and J. H. Waite, *J. Am. Chem. Soc.*, 2013, **135**, 377–383.
- 94 W. Wei, Y. Tan, N. R. Martinez Rodriguez, J. Yu, J. N. Israelachvili and J. H. Waite, *Acta Biomater.*, 2014, **10**, 1663–1670.
- 95 S. Kim, H. Y. Yoo, J. Huang, Y. Lee, S. Park, Y. Park, S. Jin, Y. M. Jung, H. Zeng, D. S. Hwang and Y. Jho, *ACS Nano*, 2017, **11**, 6764–6772.
- 96 S. Kim, J. Huang, Y. Lee, S. Dutta, H. Y. Yoo, Y. M. Jung, Y. Jho, H. Zeng and D. S. Hwang, *Proc. Natl. Acad. Sci.*, 2016, **113**, E847–E853.
- 97 B. K. Ahn, *J. Am. Chem. Soc.*, 2017, **139**, 10166–10171.
- 98 J. Saiz-Poseu, J. Mancebo-Aracil, F. Nador, F. Busqué and D. Ruiz-Molina, *Angew. Chemie - Int. Ed.*, 2019, **58**, 696–714.
- 99 H. Lee, N. F. Scherer and P. B. Messersmith, *Proc. Natl. Acad. Sci.*, 2006, **103**, 12999–13003.
- 100 J. Yu, W. Wei, E. Danner, R. K. Ashley, J. N. Israelachvili and J. H. Waite, *Nat. Chem. Biol.*, 2011, **7**, 588–590.
- 101 E. W. Danner, Y. Kan, M. U. Hammer, J. N. Israelachvili and J. H. Waite, *Biochemistry*, 2012, **51**, 6511–6518.
- 102 S. C. T. Nicklisch, J. E. Spahn, H.J. Zhou, C.M. Gruian and J. H. Waite, *Biochemistry*, 2016, **55**, 2022–2030.
- 103 J. H. Ryu, P. B. Messersmith and H. Lee, *ACS Appl. Mater. Interfaces*, 2018, **10**, 7523–7540.
- 104 Y. J. Xu, K. Wei, P. Zhao, Q. Feng, C. K. K. Choi and L. Bian, *Biomater. Sci.*, 2016, **4**, 1726–1730.
- 105 M. J. Harrington, A. Masic, N. Holten-Andersen, J. H. Waite and P. Fratzl, *Science*, 2010, **328**, 216–220.

- 106 M. J. Sever, J. T. Weisser, J. Monahan, S. Srinivasan and J. J. Wilker, *Angew. Chemie - Int. Ed.*, 2004, **43**, 448–450.
- 107 B. P. Lee, A. Narkar and R. Wilharm, *Sensors Actuators, B Chem.*, 2016, **227**, 248–254.
- 108 L. He, D. E. Fullenkamp, J. G. Rivera and P. B. Messersmith, *Chem. Commun.*, 2011, **47**, 7497–7499.
- 109 W. Zhao and Y. Wang, *Adv. Colloid Interface Sci.*, 2017, **239**, 199–212.
- 110 W. Wei, L. Petrone, Y. Tan, H. Cai, J. N. Israelachvili, A. Miserez and J. H. Waite, *Adv. Funct. Mater.*, 2016, **26**, 3496–3507.
- 111 B. Yang, S. Jin, Y. Park, Y. M. Jung and H. J. Cha, *Small*, 2018, **14**, 1803377.
- 112 M. A. Gebbie, W. Wei, A. M. Schrader, T. R. Cristiani, H. A. Dobbs, M. Idso, B. F. Chmelka, J. H. Waite and J. N. Israelachvili, *Nat. Chem.*, 2017, **9**, 473–479.
- 113 M. V Rapp, G. P. Maier, H. A. Dobbs, N. J. Higdon, J. H. Waite, A. Butler and J. N. Israelachvili, *J. Am. Chem. Soc.*, 2016, **138**, 9013–9016.
- 114 M. Shin, K. Kim, W. Shim, J. W. Yang and H. Lee, *ACS Biomater. Sci. Eng.*, 2016, **2**, 687–696.
- 115 K. Kim, M. Shin, M. Y. Koh, J. H. Ryu, M. S. Lee, S. Hong and H. Lee, *Adv. Funct. Mater.*, 2015, **25**, 2402–2410.
- 116 L. M. McDowell, L. A. Burzio, J. H. Waite and J. Schaefer, *J. Biol. Chem.*, 1999, **274**, 20293–20295.
- 117 H. G. Silverman and F. F. Roberto, *Mar. Biotechnol.*, 2007, **9**, 661–681.
- 118 B. P. Lee, J. L. Dalsin and P. B. Messersmith, *Biomacromolecules*, 2002, **3**, 1038–1047.
- 119 M. A. North, C. A. Del Grosso and J. J. Wilker, *ACS Appl. Mater. Interfaces*, 2017, **9**, 7866–7872.
- 120 B. K. Ahn, S. Das, R. Linstadt, Y. Kaufman, N. R. Martinez-Rodriguez, R. Mirshafian, E. Kesselman, Y. Talmon, B. H. Lipshutz, J. N. Israelachvili and J. H. Waite, *Nat. Commun.*, 2015, **6**, 8663.
- 121 Y. Zhou, J. Zhao, X. Sun, S. Li, X. Hou, X. Yuan and X. Yuan, *Biomacromolecules*, 2016, **17**, 622–630.
- 122 W. Cheng, X.W. Zeng, H.Z. Chen, Z.M. Li, W.F. Zeng, L. Mei and Y. L. Zhao, *ACS Nano*, 2019, **13**, 8537–8565
- 123 Y. Liu, K. Ai and L. Lu, *Chem. Rev.*, 2014, **114**, 5057–5115.
- 124 M. E. Lyngø, R. van der Westen, A. Postma and B. Stadler, *Nanoscale*, 2011, **3**, 4916–4928.
- 125 H. Meng, J. Gazella and B. P. Lee, in *Bio- and Bioinspired Nanomaterials eds. D. Ruiz-Molina, F. Novio and C. Roscini*, Wiley-VCN, Weinheim, Germany, **2014**, pp. 309–334.
- 126 L. Han, M. Wang, P. Li, D. Gan, L. Yan, J. Xu, K. Wang, L. Fang, C. W. Chan, H. Zhang, H. Yuan and X. Lu, *ACS Appl. Mater. Interfaces*, 2018, **10**, 28015–28026.
- 127 W. Zhu, J. Iqbal and D. A. Wang, *J. Mater. Chem. B*, 2019, **7**, 1741–1752.
- 128 W. Zhang, Z. Pan, F. K. Yang and B. Zhao, *Adv. Funct. Mater.*, 2015, **25**, 1588–1597.



- 129 L. Han, K. Liu, M. Wang, K. Wang, L. Fang, H. Chen, J. Zhou and X. Lu, *Adv. Funct. Mater.*, 2018, **28**, 1704195.
- 130 Y. Hong, F. Zhou, Y. Hua, X. Zhang, C. Ni, D. Pan, Y. Zhang, D. Jiang, L. Yang, Q. Lin, Y. Zou, D. Yu, D. E. Arnot, X. Zou, L. Zhu, S. Zhang and H. Ouyang, *Nat. Commun.*, 2019, **10**, 2060.
- 131 B. P. Lee, P. B. Messersmith, J. N. Israelachvili and J. H. Waite, *Annu. Rev. Mater. Res.*, 2011, **41**, 99–132.
- 132 J. Saiz-Poseu, J. Sedó, B. García, C. Benaiges, T. Parella, R. Alibés, J. Hernando, F. Busqué and D. Ruiz-Molina, *Adv. Mater.*, 2013, **25**, 2066–2070.
- 133 N. F. Della Vecchia, R. Avolio, M. Alfè, M. E. Errico, A. Napolitano and M. D’Ischia, *Adv. Funct. Mater.*, 2013, **23**, 1331–1340.
- 134 Q. Ye, F. Zhou and W. Liu, *Chem. Soc. Rev.*, 2011, **40**, 4244–4258.
- 135 S. Moulay, *Polym. Rev.*, 2014, **54**, 436–513.
- 136 H. Zhang, T. Zhao, B. Newland, W. Liu, W. Wang and W. Wang, *Prog. Polym. Sci.*, 2018, **78**, 47–55.
- 137 M. Yu and T. J. Deming, *Macromolecules*, 1998, **31**, 4739–4745.
- 138 G. Westwood, T. N. Horton and J. J. Wilker, *Macromolecules*, 2007, **40**, 3960–3964.
- 139 H. J. Meredith and J. J. Wilker, *Adv. Funct. Mater.*, 2015, **25**, 5057–5065.
- 140 P. B. Messersmith and C. E. Brubaker, *Langmuir*, 2012, **28**, 2200–2205.
- 141 J. Liu and O. A. Scherman, *Adv. Funct. Mater.*, 2018, **28**, 1800848.
- 142 L. Han, L. Yan, K. Wang, L. Fang, H. Zhang, Y. Tang, Y. Ding, L. T. Weng, J. Xu, J. Weng, Y. Liu, F. Ren and X. Lu, *NPG Asia Mater.*, 2017, **9**, e372.
- 143 X. Zeng, E. Westhaus, N. Eberle, B. Lee and P. B. Messersmith, *Am. Chem. Soc. Polym. Prepr. Div. Polym. Chem.*, 2000, **41**, 989–990.
- 144 C. E. Brubaker and P. B. Messersmith, *Biomacromolecules*, 2011, **12**, 4326–4334.
- 145 B. P. Lee, J. L. Dalsin and P. B. Messersmith, *Biomacromolecules*, 2002, **3**, 1038–1047.
- 146 C. E. Brubaker, H. Kissler, L. J. Wang, D. B. Kaufman and P. B. Messersmith, *Biomaterials*, 2010, **31**, 420–427.
- 147 Y. Lee, H. J. Chung, S. Yeo, C. H. Ahn, H. Lee, P. B. Messersmith and T. G. Park, *Soft Matter*, 2010, **6**, 977–983.
- 148 J. H. Ryu, Y. Lee, W. H. Kong, T. G. Kim, T. G. Park and H. Lee, *Biomacromolecules*, 2011, **12**, 2653–2659.
- 149 K. Huang, B. P. Lee, D. R. Ingram and P. B. Messersmith, *Biomacromolecules*, 2002, **3**, 397–406.
- 150 M. Guvendiren, P. B. Messersmith and K. R. Shull, *Biomacromolecules*, 2008, **9**, 122–128.
- 151 B. P. Lee, C. Y. Chao, F. Nelson Nunalee, E. Motan, K. R. Shull and P. B. Messersmith, *Macromolecules*, 2006, **39**, 1740–1748.
- 152 H. Chung, P. Glass, J. M. Pothen, M. Sitti and N. R. Washburn, *Biomacromolecules*, 2011, **12**, 342–347.
- 153 H. Zhang, T. Zhao, B. Newland, P. Duffy, A. N. Annaidh, E. D. O’Cearbhaill and W.

- Wang, *J. Mater. Chem. B*, 2015, **3**, 6420–6428.
- 154 N. Holten-Andersen, M. J. Harrington, H. Birkedal, B. P. Lee, P. B. Messersmith, K. Y. C. Lee and J. H. Waite, *Proc. Natl. Acad. Sci. U. S. A.*, 2011, **108**, 2651–2655.
- 155 N. Holten-Andersen, A. Jaishankar, M. J. Harrington, D. E. Fullenkamp, G. Dimarco, L. He, G. H. McKinley, P. B. Messersmith and K. Y. C. Lee, *J. Mater. Chem. B*, 2014, **2**, 2467–2472.
- 156 Z. Shafiq, J. Cui, L. Pastor-Pérez, V. San Miguel, R. A. Gropeanu, C. Serrano and A. Del Campo, *Angew. Chemie - Int. Ed.*, 2012, **51**, 4332–4335.
- 157 A. Cholewinski, F. (kuo) Yang and B. Zhao, *Mater. Horizons*, 2019, **6**, 285–293.
- 158 P. Glass, H. Chung, N. R. Washburn and M. Sitti, *Langmuir*, 2009, **25**, 6607–6612.
- 159 P. Glass, H. Chung, N. R. Washburn and M. Sitti, *Langmuir*, 2010, **26**, 17357–17362.
- 160 H. Yi, S. H. Lee, M. Seong, M. K. Kwak and H. E. Jeong, *J. Mater. Chem. B*, 2018, **6**, 8064–8070.
- 161 A. R. Narkar, C. Kendrick, K. Bellur, T. Leftwich, Z. Zhang and B. P. Lee, *Soft Matter*, 2019, **15**, 5474–5482.
- 162 A. R. Narkar, B. Barker, M. Clisch, J. Jiang and B. P. Lee, *Chem. Mater.*, 2016, **28**, 5432–5439.
- 163 H. Yuk, T. Zhang, G. A. Parada, X. Liu and X. Zhao, *Nat. Commun.*, 2016, **7**, 1–11.
- 164 T. Chen, Y. Chen, H. U. Rehman, Z. Chen, Z. Yang, M. Wang, H. Li and H. Liu, *ACS Appl. Mater. Interfaces*, 2018, **10**, 33523–33531.
- 165 E. Park, J. Lee, K. M. Huh, S. H. Lee and H. Lee, *Adv. Healthcare Mater.*, 2019, **8**, 1900275.
- 166 M. Shin, S.-G. Park, B.-C. Oh, K. Kim, S. Jo, M. S. Lee, S. S. Oh, S.-H. Hong, E.-C. Shin, K.-S. Kim, S.-W. Kang and H. Lee, *Nat. Mater.*, 2016, **16**, 147.
- 167 C. Haller, W. Buerzle, C. Brubaker, P. Messersmith, E. Mazza, N. Ochsenein-Koelble, R. Zimmermann and M. J. P. d. Ehrbar, *Prenat. Diagn.*, 2011, **31**, 654–660.
- 168 A. Kivelio, P. DeKoninck, M. Perrini, C. E. Brubaker, P. B. Messersmith, E. Mazza, J. Deprest, R. Zimmermann, M. Ehrbar and N. Ochsenein-Koelble, *European Journal of Obstetrics & Gynecology and Reproductive Biology*, 2013, **171**, 240–245.
- 169 S. Liang, Y. Zhang, H. Wang, Z. Xu, J. Chen, R. Bao, B. Tan, Y. Cui, G. Fan and W. Wang, *Adv. Mater.*, 2018, **30**, 1704235.
- 170 R. Wang, J. Li, W. Chen, T. Xu, S. Yun, Z. Xu, Z. Xu, T. Sato, B. Chi and H. Xu, *Adv. Funct. Mater.*, 2017, **27**, 1604894.
- 171 L. Li, B. Yan, J. Yang, L. Chen and H. Zeng, *Adv. Mater.*, 2015, **27**, 1294–1299.
- 172 L. Li, B. Yan, J. Yang, W. Huang, L. Chen and H. Zeng, *ACS Appl. Mater. Interfaces*, 2017, **9**, 9221–9225.
- 173 J. Guo, W. Wang, J. Hu, D. Xie, E. Gerhard, M. Nisic, D. Shan, G. Qian, S. Zheng and J. Yang, *Biomaterials*, 2016, **85**, 204–217.

- 174 A. GhavamiNejad, C. H. Park and C. S. Kim, *Biomacromolecules*, 2016, **17**, 1213-1223.
- 175 H. Meng, P. K. Forooshani, P. U. Joshi, J. Osborne, X. Mi, C. Meingast, R. Pinnaratip, J. Kelley, A. Narkar, W. He, M. C. Frost, C. L. Heldt and B. P. Lee, *Acta Biomater.*, 2019, **83**, 109-118.
- 176 L. García-Fernández, J. Cui, C. Serrano, Z. Shafiq, R. A. Gropeanu, V. S. Miguel, J. I. Ramos, M. Wang, G. K. Auernhammer, S. Ritz, A. A. Golriz, R. Berger, M. Wagner and A. d. Campo, *Adv. Mater.*, 2013, **25**, 529-533.
- 177 J. Guo, W. Sun, J. P. Kim, X. Lu, Q. Li, M. Lin, O. Mrowczynski, E. B. Rizk, J. Cheng, G. Qian and J. Yang, *Acta Biomater.*, 2018, **72**, 35-44.
- 178 J. Xu, M. Tam, S. Samaei, S. Lerouge, J. Barralet, M. M. Stevenson and M. Cerruti, *Acta Biomater.*, 2017, **48**, 247-257.
- 179 Y. Liang, X. Zhao, P. X. Ma, B. Guo, Y. Du and X. Han, *J. Colloid Interface Sci.*, 2019, **536**, 224-234.
- 180 J. Xu, S. Strandman, J. X. X. Zhu, J. Barralet and M. Cerruti, *Biomaterials*, 2015, **37**, 395-404.
- 181 C. J. Kastrup, M. Nahrendorf, J. L. Figueiredo, H. Lee, S. Kambhampati, T. Lee, S.-W. Cho, R. Gorbатов, Y. Iwamoto, T. T. Dang, P. Dutta, J. H. Yeon, H. Cheng, C. D. Pritchard, A. J. Vegas, C. D. Siegel, S. MacDougall, M. Okonkwo, A. Thai, J. R. Stone, A. J. Coury, R. Weissleder, R. Langer and D. G. Anderson, *Proc. Natl. Acad. Sci. U.S.A.*, 2012, **109**, 21444-21449.
- 182 A. GhavamiNejad, M. SamariKhalaj, L. E. Aguilar, C. H. Park and C. S. Kim, *Sci. Rep.*, 2016, **6**, 33594.
- 183 W. J. Yang, P. Zhou, L. Liang, Y. Cao, J. Qiao, X. Li, Z. Teng and L. Wang, *ACS Appl. Mater. Interfaces*, 2018, **10**, 18560-18573.
- 184 J. Cui, Y. Wang, A. Postma, J. Hao, L. Hosta-Rigau and F. Caruso, *Adv. Funct. Mater.*, 2010, **20**, 1625-1631.
- 185 C. J. Ochs, T. Hong, G. K. Such, J. Cui, A. Postma and F. Caruso, *Chem. Mater.*, 2011, **23**, 3141-3143.
- 186 J. Cui, Y. Yan, G. K. Such, K. Liang, C. J. Ochs, A. Postma and F. Caruso, *Biomacromolecules*, 2012, **13**, 2225-2228.
- 187 Y. Ju, J. Cui, H. Sun, M. Müllner, Y. Dai, J. Guo, N. Bertleff-Zieschang, T. Suma, J. Richardson and F. Caruso, *Biomacromolecules*, 2016, **17**, 2268-2276.
- 188 C. Lee, J. Shin, J. S. Lee, E. Byun, J. H. Ryu, S. H. Um, D.-I. Kim, H. Lee and S.-W. Cho, *Biomacromolecules*, 2013, **14**, 2004-2013.
- 189 S. Hong, K. Yang, B. Kang, C. Lee, I. T. Song, E. Byun, K. I. Park, S.-W. Cho and H. Lee, *Adv. Funct. Mater.*, 2013, **23**, 1774-1780.
- 190 J. Shin, J. S. Lee, C. Lee, H.-J. Park, K. Yang, Y. Jin, J. H. Ryu, K. S. Hong, S.-H. Moon, H.-M. Chung, H. S. Yang, S. H. Um, J.-W. Oh, D.-I. Kim, H. Lee and S.-W. Cho, *Adv. Funct. Mater.*, 2015, **25**, 3814-3824.

- 191 H.-J. Park, Y. Jin, J. Shin, K. Yang, C. Lee, H. S. Yang and S.-W. Cho, *Biomacromolecules*, 2016, **17**, 1939-1948.
- 192 C. DiMaggio, P. Ayoung-Chee, M. Shinseki, C. Wilson, G. Marshall, D. C. Lee, S. Wall, S. Maulana, H. L. Pachter and S. Frangos, *Injury*, 2016, **47**, 1393-1403.
- 193 M. P. Rowan, L. C. Cancio, E. A. Elster, D. M. Burmeister, L. F. Rose, S. Natesan, R. K. Chan, R. J. Christy and K. K. Chung, *Crit. Care*, 2015, **19**, 243.
- 194 Y. Chee, J. Crawford, H. Watson and M. Greaves, *Br. J. Haematol.*, 2008, **140**, 496-504.
- 195 M. C. Bélanger and Y. Marois, *J. Biomed. Mater. Res. A*, 2001, **58**, 467-477.
- 196 R. Pinnaratip, M. S. A. Bhuiyan, K. Meyers, R. M. Rajachar and B. P. Lee, *Adv. Healthcare Mater.*, 2019, 1801568.
- 197 J. L. Drury and D. J. Mooney, *Biomaterials*, 2003, **24**, 4337-4351.
- 198 P. Monagle and P. Massicotte, *Semin. Fetal. Neonat. M.*, 2011, **16**, 294-300.
- 199 M. E. Doerfler, B. Kaufman and A. S. Goldenberg, *Chest*, 1996, **110**, 185-188.
- 200 A. Srivastava, A. Brewer, E. Mauser-Bunschoten, N. Key, S. Kitchen, A. Llinas, C. Ludlam, J. Mahlangu, K. Mulder and M. Poon, *Haemophilia*, 2013, **19**, e1-e47.
- 201 H. S. Whang, W. Kirsch, Y. H. Zhu, C. Z. Yang and S. M. Hudson, *J. Macromol. Sci. Polym. Rev.*, 2005, **45**, 309-323.
- 202 T.-C. Chou, E. Fu, C.-J. Wu and J.-H. Yeh, *Biochem. Biophys. Res. Commun.*, 2003, **302**, 480-483.
- 203 E. Caló and V. V. Khutoryanskiy, *Eur. Polym. J.*, 2015, **65**, 252-267.
- 204 H. Mogami, A. H. Kishore, Y. Akgul and R. A. Word, *Sci. Rep.*, 2017, **7**, 13139.
- 205 A. Kivelio, P. DeKoninck, M. Perrini, C. E. Brubaker, P. B. Messersmith, E. Mazza, J. Deprest, R. Zimmermann, M. Ehrbar and N. Ochsenein-Koelble, *Eur. J. Obstet. Gynecol. Reprod. Biol.*, 2013, **171**, 240-245.
- 206 C. Haller, W. Buerzle, A. Kivelio, M. Perrini, C. Brubaker, R. Gubeli, A. Mallik, W. Weber, P. Messersmith and E. Mazza, *Acta Biomater.*, 2012, **8**, 4365-4370.
- 207 G. Bilic, C. Brubaker, P. B. Messersmith, A. S. Mallik, T. M. Quinn, C. Haller, E. Done, L. Gucciardo, S. M. Zeisberger and R. Zimmermann, *Am. J. Obstet. Gynecol.*, 2010, **202**, 85. e81-85. e89.
- 208 E. J. Benjamin, P. Muntner and M. S. Bittencourt, *Circulation*, 2019, **139**, e56-e528.
- 209 T. Anzai, *Circ. J.*, 2013, **77**, 580-587.
- 210 R. J. Aragon and N. L. Solomon, *J. Gastrointest. Oncol.*, 2012, **3**, 28-40.
- 211 A. Dhawan, J. Puppi, R. D. Hughes and R. R. Mitry, *Nat. Rev. Gastroenterol. Hepatol.*, 2010, **7**, 288-298.
- 212 M. T. De Boer, E. A. Boonstra, T. Lisman and R. J. Porte, *Digest. Surg.*, 2012, **29**, 54-61.
- 213 G. Ramage, J. P. Martínez and J. L. López-Ribot, *FEMS Yeast Res.*, 2006, **6**, 979-986.

- 214 D. Church, S. Elsayed, O. Reid, B. Winston and R. Lindsay, *Clin. Microbiol. Rev.*, 2006, **19**, 403-434.
- 215 J. L. Dalsin, L. Lin, S. Tosatti, J. Voeroes, M. Textor and P. B. Messersmith, *Langmuir*, 2005, **21**, 640-646.
- 216 J. L. Dalsin, B.-H. Hu, B. P. Lee and P. B. Messersmith, *J. Am. Chem. Soc.*, 2003, **125**, 4253-4258.
- 217 J. L. Dalsin, D. L. Sherman, B. P. Lee and P. B. Messersmith, *Polym. Mater. Sci. Eng.*, 2006, **94**, 854-855.
- 218 A. Pechey, C. N. Elwood, G. R. Wignall, J. L. Dalsin, B. P. Lee, M. Vanjecek, I. Welch, R. Ko, H. Razvi and P. A. Cadieux, *J. Urol.*, 2009, **182**, 1628-1636.
- 219 X. Liu, L. Yuan, D. Li, Z. Tang, Y. Wang, G. Chen, H. Chen and J. L. Brash, *J. Mater. Chem. B*, 2014, **2**, 5718-5738.
- 220 M. C. Stensberg, Q. Wei, E. S. McLamore, D. M. Porterfield, A. Wei and M. S. Sepúlveda, *Nanomedicine*, 2011, **6**, 879-898.
- 221 J. L. Clement and P. S. Jarrett, *Met. Based Drugs*, 1994, **1**, 467-482.
- 222 S. M. Lee, K. C. Song and B. S. Lee, *Korean J. Chem. Eng.*, 2010, **27**, 688-692.
- 223 X. Ding, G. K. Vegesna, H. Meng, A. Winter and B. P. Lee, *Macromol. Chem. Phys.*, 2015, 216, 1109-1119.
- 224 Y. Liu and B. P. Lee, *J. Mater. Chem. B*, 2016, 4, 6534-6540.
- 225 P. K. Forooshani, H. Meng and B. P. Lee, in *Advances in Bioinspired and Biomedical Materials Volume 1*, American Chemical Society, 2017, vol. 1252, ch. 10, pp. 179-196.
- 226 H. Meng, Y. Li, M. Faust, S. Konst and B. P. Lee, *Acta Biomater.*, 2015, **17**, 160-169.
- 227 H. Meng, Y. Liu and B. P. Lee, *Acta Biomater.*, 2017, **48**, 144-156.
- 228 M. Cencer, M. Murley, Y. Liu and B. P. Lee, *Biomacromolecules*, 2015, **16**, 404-410.
- 229 M. M. Cencer, Y. Liu, A. Winter, M. Murley, H. Meng and B. P. Lee, *Biomacromolecules*, 2014, **15**, 2861-2869.
- 230 C. J. Sun, A. Srivastava, J. R. Reifert and J. H. Waite, *J. Adhes.*, 2009, **85**, 126-138.
- 231 J. M. Gu, J. R. Robinson and S. H. S. Leung, *Crit. Rev. Ther. Drug.*, 1988, **5**, 21-67.
- 232 I. A. Sogias, A. C. Williams and V. V. Khutoryanskiy, *Biomacromolecules*, 2008, **9**,
- 233 J. D. Byrne, T. Betancourt and L. Brannon-Peppas, *Adv. Drug Deliv. Rev.*, 2008, **60**, 1615-1626.
- 234 A. Sosnik, J. das Neves and B. Sarmiento, *Prog. Polym. Sci.*, 2014, **39**, 2030-2075.
- 235 N. D. Catron, H. Lee and P. B. Messersmith, *Biointerphases*, 2006, **1**, 134-141.
- 236 J. Wu, L. Zhang, Y. Wang, Y. Long, H. Gao, X. Zhang, N. Zhao, Y. Cai and J. Xu, *Langmuir*, 2011, 27, 13684-13691.
- 237 J. Adams, M. Behnke, S. Chen, A. A. Cruickshank, L. R. Dick, L. Grenier, J. M. Klunder, Y.-T. Ma, L. Plamondon and R. L. Stein, *Bioorg. Med. Chem. Lett.*, 1998, **8**, 333-338.

- 238 J. Su, F. Chen, V. L. Cryns and P. B. Messersmith, *J. Am. Chem. Soc.*, 2011, **133**, 11850-11853.
- 239 Y.-J. Pan, Y.-Y. Chen, D.-R. Wang, C. Wei, J. Guo, D.-R. Lu, C.-C. Chu and C.-C. Wang, *Biomaterials*, 2012, **33**, 6570-6579.
- 240 W. J. Yang, T. Zhao, P. Zhou, S. Chen, Y. Gao, L. Liang, X. Wang and L. Wang, *Polym. Chem.*, 2017, **8**, 3056-3065.
- 241 S. De Koker, R. Hoogenboom and B. G. De Geest, *Chem. Soc. Rev.*, 2012, **41**, 2867-2884.
- 242 H. Ejima, J. J. Richardson, K. Liang, J. P. Best, M. P. Van Koeverden, G. K. Such, J. Cui and F. Caruso, *Science*, 2013, **341**, 154-157.
- 243 J. Guo, Y. Ping, H. Ejima, K. Alt, M. Meissner, J. J. Richardson, Y. Yan, K. Peter, D. von Elverfeldt, C. E. Hagemeyer and F. Caruso, *Angew. Chem.*, 2014, **126**, 5652-5657.
- 244 Y. Ping, J. Guo, H. Ejima, X. Chen, J. J. Richardson, H. Sun and F. Caruso, *Small*, 2015, **11**, 2032-2036.
- 245 A. Murua, A. Portero, G. Orive, R. M. Hernández, M. de Castro and J. L. Pedraz, *J. Control. Release*, 2008, **132**, 76-83.
- 246 X. Yang, G. Liu, L. Peng, J. Guo, L. Tao, J. Yuan, C. Chang, Y. Wei and L. Zhang, *Adv. Funct. Mater.*, 2017, **27**, 1703174.
- 247 J. Baier Leach, K. A. Bivens, C. W. Patrick Jr and C. E. Schmidt, *Biotechnol. Bioeng.*, 2003, **82**, 578-589.
- 248 J. A. Burdick and G. D. Prestwich, *Adv. Mater.*, 2011, **23**, H41-H56.
- 249 K. Y. Lee and D. J. Mooney, *Chem. Rev.*, 2001, **101**, 1869-1880.
- 250 M. Parlato, S. Reichert, N. Barney and W. L. Murphy, *Macromol. Biosci.*, 2014, **14**, 687-698.
- 251 N. Huebsch, P. R. Arany, A. S. Mao, D. Shvartsman, O. A. Ali, S. A. Bencherif, J. Rivera-Feliciano and D. J. Mooney, *Nat. Mater.*, 2010, **9**, 518.
- 252 N. E. Fedorovich, M. H. Oudshoorn, D. van Geemen, W. E. Hennink, J. Alblas and W. J. A. Dhert, *Biomaterials*, 2009, **30**, 344-353.
- 253 B. Zhao, Z.G. Gao, Y.C. Zheng and C. Gao, *J. Am. Chem. Soc.* 2019, **141**, 4541-4546.
- 254 T. K. Lytle, L.W. Chang, N. Markiewicz, S.L. Perry and C.E. Sing, *ACS Cent. Sci.* 2019, **5**, 709-718.
- 255 A. H. Hofman, I. A. van Hees, J. Yang and M. Kamperman, *Adv. Mater.*, 2018, **1704640**.
- 256 Y. Ma, S. Ma, Y. Wu, X. Pei, S. N. Gorb, Z. Wang, W. Liu and F. Zhou, *Adv. Mater.*, 2018, **30**, 1801595.
- 257 Y. Gao, K. Wu and Z. Suo, *Adv. Mater.*, 2019, **31**, 1806948.
- 258 R. Dong, X. Zhao, B. Guo and P. X. Ma, *ACS Appl. Mater. Interfaces*, 2016, **8**, 17138-17150.
- 259 Y. Li, H. Meng, Y. Liu and B. P. Lee, *Sci. World J.*, 2015, **2015**, 685-690.

- 260 R. Saltz, D. Sierra, D. Feldman, M. B. Saltz, A. Dimick and L. O. Vasconez, *Plast. Reconstr. Surg.*, 1991, **88**, 1005-1015.
- 261 A. E. K. Loo and B. Halliwell, *Biochem. Biophys. Res. Commun.*, 2012, **423**, 253.
- 262 Iso 10993: *Biological Evaluation of Medical Devices*. International Organization for Standardization: **2018**.

## Table of contents

This review presents insights into the fundamental challenges of wet adhesion, and the applications of catechol-functionalized hydrogels in diverse areas.

